



TECHNISCHE  
UNIVERSITÄT  
WIEN

Vienna University of Technology

D I P L O M A R B E I T

# Standardised monomeric Probes for Brightness-based Microscopy Methodologies

Zur Erlangung des akademischen Grades

**Diplom-Ingenieur**

im Rahmen des Studiums

**Biomedical Engineering**

eingereicht von

**Mauro Mellai**

Matrikelnummer 01528744

ausgeführt am Institut für Angewandte Physik

in der Arbeitsgruppe für Biophysik

der Fakultät für Physik der Technischen Universität Wien

unter der Anleitung von

Ao.Univ.-Prof. DI Dr. Techn. Gerhard Schütz

Univ.-Ass. DI Dr. Techn. Mario Brameshuber



Die approbierte gedruckte Originalversion dieser Diplomarbeit ist an der TU Wien Bibliothek verfügbar  
The approved original version of this thesis is available in print at TU Wien Bibliothek.

## Declaration of Authorship

Ich erkläre an Eides statt, dass ich die vorliegende Diplomarbeit selbstständig und ohne fremde Hilfe verfasst, andere als die angegebenen Quellen und Hilfsmittel nicht benutzt bzw. die wörtlich oder sinngemäß entnommenen Stellen als solche kenntlich gemacht habe.

The undersigned, unique author of this work, declares that the present thesis and the work presented in it has been written without any assistance from third parties. Furthermore, no sources have been used in the preparation of this thesis other than those indicated in the thesis itself.

The Author:

---

Vienna, June 2021



Die approbierte gedruckte Originalversion dieser Diplomarbeit ist an der TU Wien Bibliothek verfügbar  
The approved original version of this thesis is available in print at TU Wien Bibliothek.

# *Acknowledgements*

I wish here to express my gratitude to Professor Gerhard Schütz, Head of the Biophysics group at TU Wien, for giving me the unique opportunity to do my master's thesis within the group.

My deepest appreciation goes to Dr. Mario Brameshuber, who guided the activity patiently having always time for advices, training my thinking on the rigorous path of science. Even when, several times, this meant to sacrifice part of his weekends.

A special thanks goes to all members of the biophysics group, who made me feel welcome within the very nice atmosphere of the lab. In particular, Caroline Kopittke, Martin Fölser, Lukas Schrangl and Joshka Hellmeier for answering countless of my questions with helpful suggestions and short explanations on the fly that solved many of the big and little issues I encountered learning the lab procedures right.

This journey, a real Bildungsroman, through the streets of science would have not been possible without my family, my parents and my sister, who were far away but always present from the distance.

Last but not least, meeting Jasmin made many hard moments lighter.

Danke!



Die approbierte gedruckte Originalversion dieser Diplomarbeit ist an der TU Wien Bibliothek verfügbar  
The approved original version of this thesis is available in print at TU Wien Bibliothek.

# *Abstract*

## **Standardised monomeric Probes for Brightness-based Microscopy Methodologies**

by Mauro Mellai

Brightness analysis experiments via fluorescence microscopy are routinely conducted in today's biological and biophysical research worldwide. However, a standardised brightness reference to estimate the oligomerisation state of a protein is missing, regardless to the general awareness and its importance. This research project tried to pave the way for creating one. Two fundamental aspects were investigated: (i) if and how specific chemical binding methods linking a fluorescent dye to a protein can influence a monomer's brightness level; (ii) to determine optimal imaging conditions for recording a reliable monomer brightness distribution. The latter could be used as the starting point for a future development of a more complete reference system for higher oligomeric state of proteins. The experiments were conducted on supported lipid bilayer with three different monomeric proteins and were recorded with a fluorescence microscope using the same settings to assure comparability between the measurements taken at two different excitation laser powers. Next, image processing stages yielded the brightness of each protein for the two imaging conditions studied and estimated the relative diffusion coefficient for the proteins. A careful choice of the laser power should be the primary concern in any experiment involving brightness analysis, as it is a key factor in gathering useful data. In fact, it was observed that single-molecule signals bleach more in the centre of the region of interest than at the periphery, which strongly influences the recorded brightness distribution. In addition, a misleading or careless selection of too high imaging power could strongly alter the surface density estimation leading to incorrect scientific interpretations and conclusions. In fact, high laser power bleaches fluorescent single-molecule signals quicker plummeting statistics after the early frames very fast, poor statistics in image collection makes conclusions prone to errors. With the gained knowledge, it has become possible to define reproducible single-molecule references for brightness-based fluorescence microscopy experiments.



Die approbierte gedruckte Originalversion dieser Diplomarbeit ist an der TU Wien Bibliothek verfügbar  
The approved original version of this thesis is available in print at TU Wien Bibliothek.

# Contents

---

<b>Declaration of Authorship</b>	<b>iii</b>
<b>Acknowledgements</b>	<b>v</b>
<b>Abstract</b>	<b>vii</b>
<b>1 Introduction</b>	<b>1</b>
1.1 The importance of reference standards in research . . . . .	1
1.2 What is a monomer and the importance of a probe's oligomeric state . . . . .	3
1.3 The physics behind a supported lipid bilayer (SLB) . . . . .	7
1.4 Fluorescence microscopy . . . . .	9
1.4.1 The principle of Total Internal Reflection Fluorescence Microscopy (TIRF) . . . . .	12
1.5 Organisation of this work . . . . .	16
<b>2 Materials and Methods</b>	<b>17</b>
2.1 The protein probes utilised . . . . .	17
2.2 Preparation of Supported Lipid Bilayers . . . . .	22
2.2.1 Lipid vesicles preparation . . . . .	22
2.2.2 Creation of a SLB on a glass surface . . . . .	23
2.2.3 Preparation of the proteins to be added to the SLB . . . . .	23
2.3 Microscope system, laser and camera . . . . .	24
2.3.1 Laser power settings . . . . .	25
2.4 Data analysis with Matlab and Fiji . . . . .	26
2.4.1 Identification of the single molecule signals . . . . .	26
2.4.2 Estimation of the diffusion coefficient for the three probes. . . . .	27
2.4.3 Surface Density estimation . . . . .	28

<b>3 Results</b>	<b>31</b>
3.1 Some important chemical remarks . . . . .	32
3.2 Brightness distributions . . . . .	33
3.3 Pooling of images for better visibility. . . . .	35
3.4 How the distance from the centre affects the single molecule's brightness . . . . .	40
3.5 Estimation of the diffusion coefficient for the three probes . . . . .	42
3.6 A look back at this chapter . . . . .	44
<b>4 Discussion</b>	<b>45</b>
4.1 What the experimental findings tell us . . . . .	45
4.2 Does diffusion play a role here? . . . . .	47
4.3 Conclusions . . . . .	48
<b>Bibliography</b>	<b>49</b>



Die approbierte gedruckte Originalversion dieser Diplomarbeit ist an der TU Wien Bibliothek verfügbar  
The approved original version of this thesis is available in print at TU Wien Bibliothek.

*To my parents who were far away  
but always present from the distance...  
to my sister who was my greatest silent supporter...  
to Jasmin who made many hard moments lighter...*

*"Imparerai a tue spese che nel lungo tragitto della vita  
incontrerai tante maschere e pochi volti".  
Luigi Pirandello*



Die approbierte gedruckte Originalversion dieser Diplomarbeit ist an der TU Wien Bibliothek verfügbar  
The approved original version of this thesis is available in print at TU Wien Bibliothek.

# Chapter 1

## Introduction

---

The current research project aimed to investigate two aspects:

- if and how some commonly used chemical binding methods to link a fluorescent dye to a protein can influence a monomer's brightness.
- to determine optimal imaging conditions for recording a reliable monomer brightness distribution.

With the gained knowledge, it has become possible to define reproducible single-molecule references for brightness-based fluorescence microscopy experiments.

### 1.1 The importance of reference standards in research

In their recent article [1], Mund and Ries call for reference standards in super-resolution microscopy by emphasising that quantitative analysis of reference standard images is functional when characterising the performance of microscopes over time, as this allows objective benchmarking of newly developed microscopy and labelling techniques. Furthermore, it increases the comparability of super-resolution microscopy data between different laboratories, which helps to make e.g. research comparable over continents reducing misunderstanding of results. However, in order to obtain high quality data, conditions like sample quality, image acquisition electronics and image processing algorithms must be optimised.

This is by far not trivial in practical terms and judging the actual quality of images taken in several research laboratories with several devices and processing methods becomes challenging [2], [3]. Localisation precision is the parameter commonly chosen to describe quantitatively how precisely the position of a single molecule has been determined.

Thompson et al. [4] defined localisation precision as 'Standard Deviation of localisations around the actual position of the fluorophore'. Even though it is possible to measure localisation precision experimentally, the usual procedure is to estimate it with fitting software. However, this computational approach yields a theoretical best-case scenario, leaving the nasty question of its effective reliability open. In fact, incorrect parameters may have been utilised in the software or some instabilities could have happened during image acquisition.

As Mund and Ries highlight: 'Images and statistics from reference standard measurements provide an objective way to benchmark the performance of any microscopy pipeline' [1]. Their focus is a reference standard for molecule's position. In the same vein, single-molecule references are also needed in brightness-based experiments to study the oligomerisation state of known molecules or proteins. A prominent example of brightness-based experiments utilising single-molecule references is determining the oligomerisation state of a protein. Brightness references, in general, consist of samples with a well-defined number of fluorescent dyes. Such a sample enables the comparison of absolute intensities within one sample of unknown oligomeric state and relates the measured intensities to reference intensities in units of "absolute number of dyes" [9]. For the purpose of this thesis, the comparison of the brightness of a labelled complex with the single molecule reference will yield the number of molecules in this complex.

Furthermore, reference systems are helpful in other stoichiometry-related techniques such as Thinning Out Clusters while Conserving the Stoichiometry of Labelling (TOCCSL) [12], [13], [14] and in any brightness analyses experiment in general, independent of the technique chosen. For example, by using brightness-based experiments, the oligomerisation state of e.g. the T cell receptor was recently found to be purely monomeric [5] i.e. independent of the activation state. Accurate single-molecule brightness references, in fact, can be essential for several applications such as brightness analysis applied for characterising biochemical reactions [6] or to quantify hetero- and homo-interactions

in protein mixtures [7]. The brightness of molecular complexes is inherently proportional to their stoichiometry, i.e. the number of individual fluorescently labelled monomer forming this protein complex [7]. Another application could be in DNA origami-based structures, where proteins' stoichiometry plays a role in the spacial requirements for T cell activation [8].

To this respect, it suffices to recall what Macdonald et al. state: 'quantitative interpretation of brightness experiments relies on a calibration procedure and requires brightness standards' [10]. My focus in this thesis will be on developing a standard monomeric probe for brightness analysis since the incorrect estimation of a monomer brightness gives wrong results.

## 1.2 What is a monomer and the importance of a probe's oligomeric state

A standardised reference probe for brightness analyses yields an identical brightness signal in the images every time it is used in a microscopy system. This implies consistency in the sample preparation part and the image acquisition and imaging processing parts from the final analysed images. Such a sample, to be regarded as standard, needs to meet certain strict criteria, such as being an easy to prepare bilayer with probe molecules, and with wide applicability with a variety of labelling options.

Monovalent protein probes for standardisation offer a valid example of single-molecule probes because they carry ideally only one fluorescent marker (see Figure 1.1). The brightness  $B$  of a fluorescent dye, such as the Alexa Fluor 647 (AF647) used in this thesis, attached to a monomer counts for one molecule. When it is stoichiometrically attached to a monomeric protein by proper functionalisation methods as those discussed later, it represents a brightness reference standard for exactly one molecule, a monomer. In the same fashion, it will yield twice the brightness if attached to a dimeric protein which will accommodate two fluorescent dyes. Once the monomeric protein production process guarantees it is surely a monomer, then it can serve as a brightness reference by taking its brightness value with that fluorophore attached for calibration.

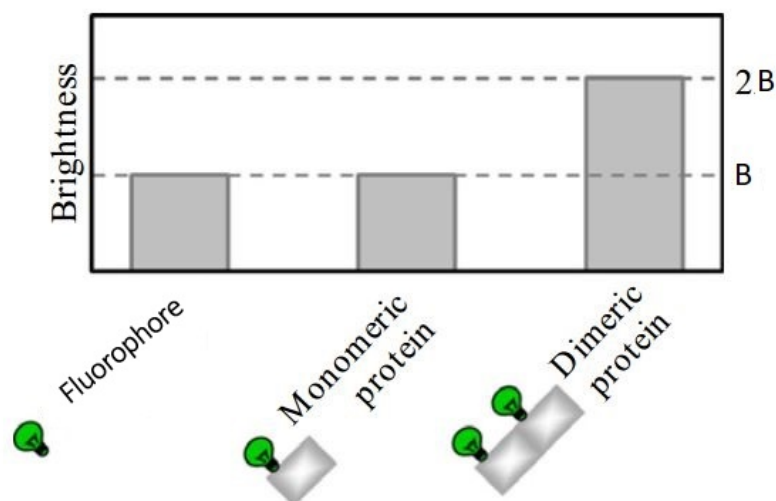
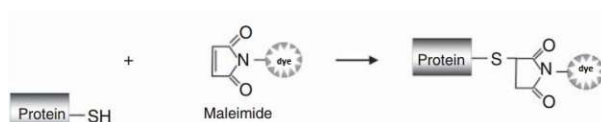


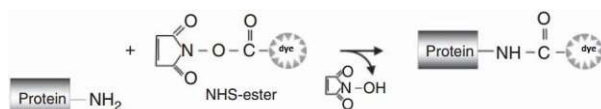
**Figure 1.1:** Brightness  $B$  of a fluorescent dye e.g. AF647 or AF488. When attached to a monomeric protein by proper functionalisation chemistry, it yields a brightness reference for a single protein. Likewise, it will yield twice the brightness if attached to a dimer protein which will accommodate two fluorochromes. Image adapted from [10]

By doing this, it allows to determine oligomerisation states of unknown molecules [11]. Of course, changing the fluorophore used would require a new calibration. A quantification of the brightness of a molecule with unknown stoichiometry becomes possible and calculating the likelihood for a dimer, a trimer, or a higher level oligomer is straightforward.

All fluorescence techniques employ fluorochrome-labelling chemistry for visualising the target [5]. Common labelling strategies are the use of a fluorescent ligand or antibody or linking the target to a fluorescent protein, the most famous example of which is the enhanced green fluorescent protein (EGFP) [20]. In this thesis, the fluorochrome of choice has been the Alexa Fluor 647 (AF647) organic dyes functionalised with amine-reactive groups such as N-hydroxysuccinimidyl ester (NHS-ester) [25] or with thiol-reactive chemical groups such as maleimide. In today's research, these two methods are widely used to link a fluorescent marker to a protein and displayed in Figure 1.2. To date, maleimide–thiol coupling still remains the biochemist's preferred method for the scalable chemical modification of proteins through cysteine residues [18]. The AF647 dye with the desired functionalisation is available for purchase from Thermofisher Scientific, similarly other companies sell a number of alternative dyes as well, e.g. di ATTO fluorophores family.



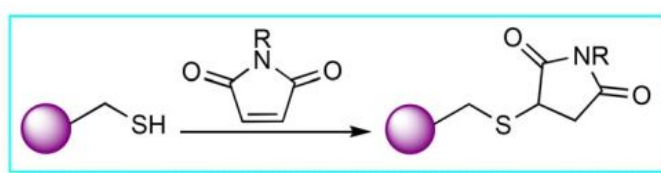
(a) Coupling of a protein with a cysteine residue -SH with Maleimide functionalisation for labelling dyes



(b) Coupling with NHS Ester functionalisation for labelling dyes

**Figure 1.2:** The two functionalisation methods used in protein probes' production. Images adapted from [21]

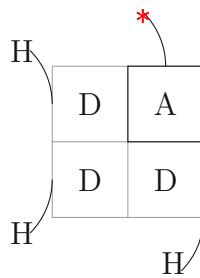
In a nutshell, "the monomeric tools" utilised for the experiments are made up of these four pieces: first the fluorescent dye bought with functionalisation group, second the tetramer streptavidin in monovalent version with or without cysteine residue depending on the scope (see chapter two and, for the actual preparation protocol, the publication [22]). Third, a biotin-lysine complex i.e. biocytin, and fourth a pMHC class II. The final results were (i) a monovalent Streptavidin with the dye site-specifically linked with maleimide functionalisation via a cysteine residue (mSav-C-AF647) as sketched in Figure 1.3, (ii) a monovalent Streptavidin where an NHS-functionalised AF647 dye was conjugated to a biocytin (biotin-lysine complex) linked to the streptavidin giving mSav-B-AF647 and (iii) a pMHC class II molecule site-specifically labelled with maleimide functionalised AF647 linked to the peptide. Details about the production protocol for pMHC can be found in [23].



R = fluorescent tags, polymers, radio labels, albumin-binding moieties, metalloenzymes, lipids, drugs

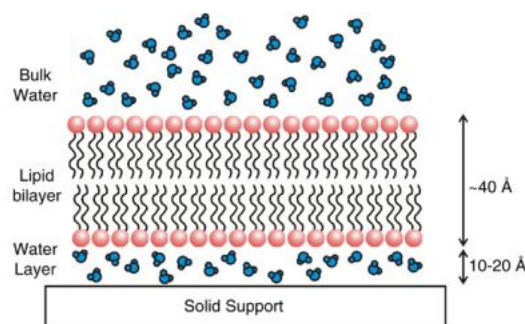
**Figure 1.3:** Scheme of cysteine-mediated protein modification via maleimide. The ball linked to sulphur indicates the protein linked to cysteine. Image taken from [18]

Figure 1.4 presents a geometrical sketch of the mSav with the biotin with fluorophore bound to the alive subunit and Histidine tags (H) on the dead subunits. In fact, to study these proteins, they were anchored via histidine-tags to nickel ions present in the supported lipid bilayer (SLB) carrying Ni-NTA lipids. The His-Tag technique takes advantage of the high affinity of  $\text{Ni}^{2+}$  ions for histidine residues of proteins [21]. In a nutshell, an His-tag is a sequence of, usually, six residues of the amino acid Histidine [15]. When added to the C-terminal end or to the N-terminal end of the protein of interest, these histidines confer the protein high affinity for bivalent nickel or cobalt ions complexed via nitrilotriacetic acid (NTA) [21].



**Figure 1.4:** Sketch of the Streptavidin tetramer made monovalent with one alive subunit A (capable of binding biotin with AF647) and the three His-tags H on the dead subunits D (unable to bind biotin)

Now, let's turn our attention to the biophysics behind the "chemical tool" chosen to make these proteins "visible" under the fluorescence microscope. Supported lipid bilayers (SLBs) are a well-known cell membrane mimics that can be formed on solid surfaces with great popularity in chemistry, biology, material science and several biomedical fields [27]. In solid supported systems such as an SLB, membrane fluidity is maintained by a 10-20 Å thick layer of water between the substrate and the bilayer as illustrated in Figure 1.5.



**Figure 1.5:** Sketch of a solid supported lipid bilayer. The membrane is separated from the glass by water layer 10-20 Å in thickness. Image taken from [27]

## 1.3 The physics behind a supported lipid bilayer (SLB)

The supported lipid bilayers (SLB) for this research were made through a method known as vesicle fusion, a common choice in today's research laboratories due to its simple handling and limited time consumption while keeping costs reasonable. In fact, preparation time from creating the vesicles to have a bilayer ready for use, takes less than an hour. Seifert and Lipowsky developed a theoretical model predicting that the bilayer formation depends on the properties of the vesicles such as bending modulus, curvature and adhesive interactions with the solid substrate [28], [29]. According to their theory, vesicle rupture will affect only the adsorbed vesicles above a critical size [30]. Figure 1.6 shows the steps that have been identified in the vesicle fusion process in several studies over the years [30], [31], [32], [33].

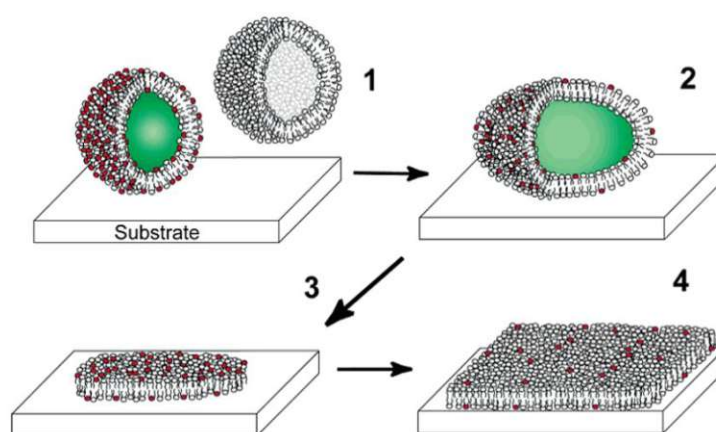


**Figure 1.6:** The four steps in SLB formation by vesicle fusion. (1) Vesicle adsorption. (2) Fusion of vesicles at surface to form larger vesicles. (3) Rupture of the fused vesicles to create bilayer disks. (4) Cooperative merging of the neighbouring vesicles leads to subsequent formation of the continuous bilayer [30].

Hence, the steps in bilayer formation result:

1. Isolated vesicle adsorption to the support surface
2. Fusion of vesicles at the surface to form larger vesicles
3. Rupture of the fused vesicles resulting in bilayer disks
4. Cooperative merging of neighbouring vesicles to form a continuous layer

Successful fusion of vesicles on glass surfaces requires treatments such as sonication of the lipid solution, which produces the small vesicles, and argon plasma cleaning of the glass substrate to make it hydrophilic. Next steps are vesicle pouring and incubation [32].

Experimental work proved the validity of Lipowsky and Seifert's theory [31] to explain the binding and stability of the surface-bound vesicles. In their model view the bilayer is seen as a 2D sheet in a 3D space [28], [29]. The balance between adhesion energy and curvature's energy in favour of adhesion gives an explanation for adsorption, deformation and rupture of isolated vesicles (see Figure 1.7A). An attempt of numerical calculations under simplified assumptions can be found in [30].

The milestone work by Zimm and Bragg in 1959 investigating cooperative transitions in 2D bilayer system [34] provided a theoretical model to understand vesicles' behaviour. Their model shows that the size of the cooperative unit is a measure of the mean number of molecules per perimeter molecule present in a given region of ordered or fluid lipid at the centre of the transition [35].

Hence, it follows that the vesicle size limits the cooperativity of the transition in the small, single-bilayer vesicles. In simple terms, cooperativity between the surface-bound vesicles to form the bilayer requires a critical vesicle coverage that leads to a stress on the vesicles sufficient to induce their fusion and following rupture (Figure 1.7B). The ruptured vesicles expose edges which are energetically unfavourable promoting then interactions with neighbour intact vesicle. Such interactions lead to the formation of the lipid bilayer (Figure 1.7C). By a propagation process the vesicles on the glass are recruited and the bilayer expands over the whole glass support (Figure 1.7D). The whole process was also directly observed via atomic force microscopy and fluorescence microscopy [30].

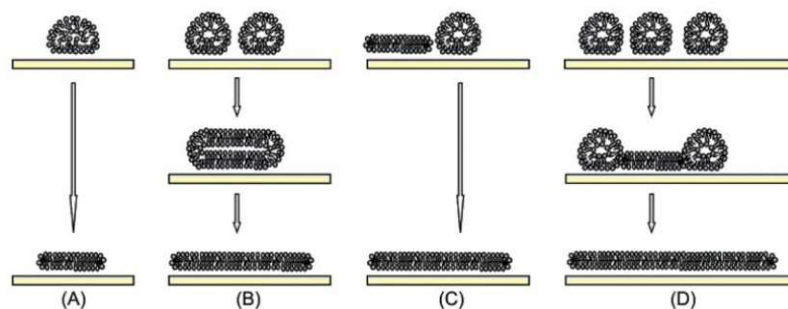


**Figure 1.7:** How vesicle's rupture works. (A) An isolated adsorbed vesicle ruptures due to support-induced energetically favourable conditions. (B) Cooperative fusion of neighbouring vesicles may end up in their rupture. (C) The ruptured vesicles' exposed edges induce rupture of the vesicles next to them. (D) At sufficient vesicle's coverage the random rupture of one triggers through its exposed lipid a rupture cascade effect which creates an extended lipid bilayer [31].

## 1.4 Fluorescence microscopy

Murphy [36] defines fluorescence as 'the emission of photons by atoms or molecules whose electrons are transiently stimulated to a higher excitation state by radiant energy from an outside source'. These atoms or molecules acting as emitters of photons are named fluorophores, such as the Alexa Fluor 647 dye which emission and absorption spectra are depicted in Figure 1.8, other examples are Alexa Fluor 488, Atto 488 etc. When a photon of appropriate wavelength  $\lambda$  hits the fluorophore, it is absorbed with a certain probability. The molar extinction coefficient  $\epsilon$  gives the probability in units of  $\text{M}^{-1}\text{cm}^{-1}$  that the fluorophore absorbs a photon. The excited molecule will emit another photon with higher wavelength i.e. lower energy. This loss of energy is a consequence of vibrational processes resulting from the oscillations between the orbitals as the electrons redistribute. Figure 1.9 shows the Jablonsky diagram, which is a simplified graphical representation of the situation at atomic level. When fluorophores come into contact with incident photons, all of the photon energy is transferred.

The difference between excitation wavelength and emission wavelength is called Stokes shift after its discoverer George G. Stokes. This shift is crucial in fluorescence microscopy where fluorescent dyes exhibiting a large Stokes shift are advantageous [36]. In fact, the larger the Stokes shift is, the lower the overlapping between absorption and emission spectra becomes. This makes it easier to isolate the emission part from the excitation part using interference filters. If emission and excitation are better separated, it is easier to define

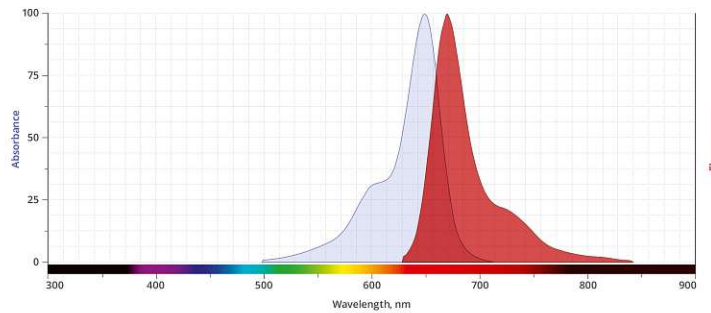


**Figure 1.8:** The spectrum of the Alexa Fluor 647 dye used in this thesis. The difference between the peaks' wavelength is called Stokes shift and its relevance is explained in the text. Image created with the spectra viewer on [www.thermofisher.com](http://www.thermofisher.com)

a more efficient detection systems, which results in a larger photon budget, maybe lower excitation times, etc. All these aspects guide in selecting the fluorescent dye for the planned experiment and the dichroic mirror to mount in the microscope. To sum up, the energy of the photons can be calculated through the famous equation  $E = h \frac{c}{\lambda}$  where  $h$  is the Planck's constant,  $c$  represents the speed of light in vacuum and  $\lambda$  is the wavelength of light in vacuum. Hence, the energy difference between incident and emitted photon is:

$$\Delta E_{\text{ph}} = E_{\text{in}} - E_{\text{em}} = hc \left( \frac{1}{\lambda_{\text{in}}} - \frac{1}{\lambda_{\text{em}}} \right)$$

This phenomenon of fluorescence yields a better chemical contrast by using fluorescent molecules in a technique named fluorescence microscopy. In this vein, observing microscopical 'objects', so far unnoticeable becomes possible. Since this  $\lambda$  shift takes place in the visual portion of the electromagnetic spectrum, the emitted  $\lambda$  corresponds to a colour for the human retina. The use of fluorochromes is common in many biomedical fields. One interesting application is in the quest for antigens e.g. bacteria on objects' surfaces. The process involves a fluorochrome, which is attached to an antibody sensitive to the specific bacterium one wants to detect, making the antibody fluorescent. Next, the surface to be tested for bacterial contamination or similar (like the anthrax spores occasionally on the news) is sampled, for instance by using some adhesive tape and sent to a laboratory. If the suspect bacterium is actually present, by adding the now-fluorescent antibody on the tape and observing under the microscope, the antibodies will group around the bacteria making them detectable by fluorescence. The high specificity of the antigen-antibody reaction guarantees a high level of correct identifications. Several other examples could be easily found in medicine or biology.

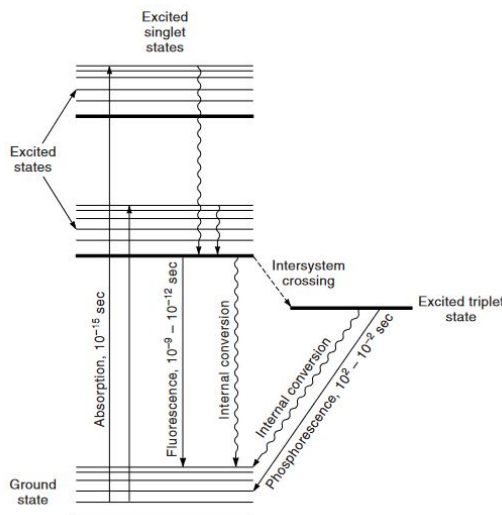


**Figure 1.9:** Jablonsky diagrams are pictorial representations of the energy states occupied by an excited electron within a fluorescent molecule. As incident photons with sufficient energy hit the fluorophores in the ground state, the electrons absorb energy becoming promoted to an excited state. This upgrade is only temporary and the electron will soon fall down to a lower energy state again. For this transition, it emits a photon of higher wavelength than the absorbed one. Image taken from [36]

Any fluorescence microscope (see Figure 1.10) works by selectively filtering the light to excite the sample, e.g. using laser light source of desired colour, and subsequently isolating the lower-energetic emitted light i.e. the fluorescence coming from the sample, through a second filter [37]. This allows for high-contrast imaging with high sensitivity [39].

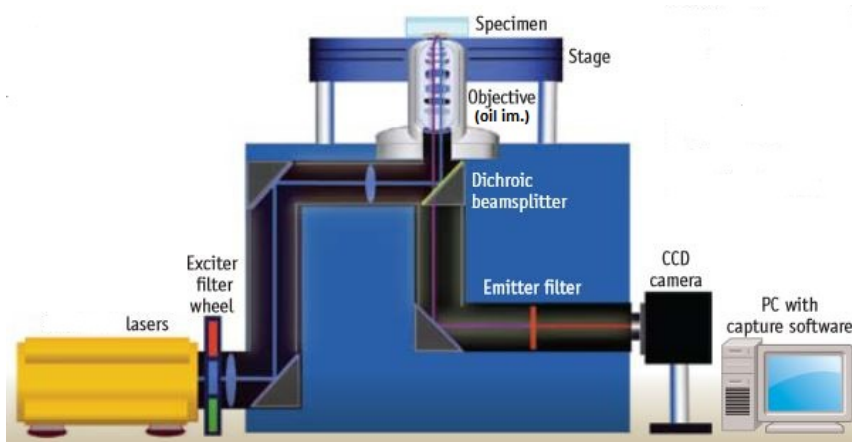


**Figure 1.10:** Sketch of an inverted microscope showing light path, filters and other important parts. Image adapted from [38].

The main drawbacks of fluorescence microscopy are photobleaching of dyes, toxicity of dyes and limited spatial resolution of recorded images [21]. Of these three, the first one assumes a primary role in the present research. Therefore, photobleaching deserves few words starting from its definition: 'photobleaching is the process of a loss of fluorescence intensity by the specimen arising from interaction between the exciting light and the fluorescent compound [21]. This unavoidable damaging of dyes occurs during the experiment affecting final image quality and, consequently, also the brightness estimated via dedicated computer programmes which is the goal of the current thesis. Optimising the intensity of exciting light and recording settings help significantly in keeping the nasty phenomenon under control. However, a handful of techniques like, for instance, Fluorescent recovery after photobleaching (FRAP) [26] or Photoactivated localisation microscopy (PALM) [25] converted this issue into an advantage, proving the ways of science to be unpredictable.

### 1.4.1 The principle of Total Internal Reflection Fluorescence Microscopy (TIRF)

The famous Snell's law governs the behaviour of light rays at the interface between two media with  $n_1 > n_2$ . When a beam of light passes from a medium 1 to medium 2 with refractive indices  $n_1 > n_2$  then part of the beam is transmitted and part is reflected. The greater the angle of incidence  $\vartheta_1$  is, the greater the reflected part of the beam gets.

Snell's law states:

$$n_1 \sin \vartheta_1 = n_2 \sin \vartheta_2$$

There are three possible cases to consider depending on the angle of incidence  $\vartheta_1$  as in Figure 1.11. It is clear that it exists a certain angle of incidence  $\vartheta_1 = \vartheta_c$ , known as the 'critical angle' at which the transmitted ray travels along the interface i.e. when  $\vartheta_2 = 90$  (Figure 1.11b). In this condition Snell says that:

$$n_1 \sin \vartheta_c = n_2 \sin 90$$

$$\vartheta_c = \sin^{-1} \left( \frac{n_2}{n_1} \right)$$

Figure 1.11a shows the case for  $\vartheta_1 < \vartheta_c$ . The interesting case in microscopy is for angle of incidence greater than the critical angle  $\vartheta_1 > \vartheta_c$  known as total internal reflection condition in which light rays are totally reflected back into the first medium (Figure 1.11c).

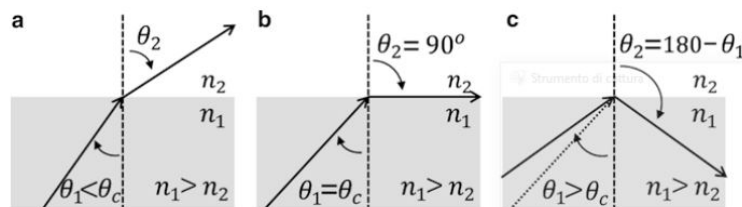


**Figure 1.11:** The situation at the interface between two media with refractive index  $n_1 > n_2$  for different angles of incidence  $\vartheta_1$ . (a) The angle of incidence is less than the critical angle. (b) The angle of incidence is equal to the critical angle. (c) The angle of incidence is greater than the critical angle. Image taken from [40]

The Fresnel equations are needed to know about the portion of light reflected and transmitted from the boundary. Without entering in mathematical details available in many optics books such as [44] or [45], by solving Fresnel's equations for the case of total internal reflection in Figure 1.11c, they show that, although light is totally reflected, there is still an electric field which crosses the boundary i.e. there is still a light wave in the second medium [44]. With respect to fluorescence microscopy, this wave can excite the fluorophores inside the sample for some 100 nm counting the distance perpendicularly to the interface. however, further away than this distance, also called penetration depth, the fluorophores are not excited anymore. To this wave is given the name of evanescent wave, and its intensity decays exponentially with perpendicular distance from the boundary (see Figure 1.12) according to the following equation:

$$I_z = I_0 \exp\left(-\frac{z}{d}\right)$$

where  $I_z$  is the field intensity at distance  $z$  from the interface,  $d$  is the decay constant of the field, and  $I_0$  is the intensity of the field at the interface i.e. at  $z=0$  as illustrated in Figure 1.12.

Penetration depth  $d$  in Figure 1.12 is given by the expression:

$$d = \frac{\lambda_{\text{ex}}}{4\pi\sqrt{n_2^2\sin^2\vartheta_1 - n_1^2}}$$

This equation [41] tells that the penetration depth is dependent on (i) the wavelength of the excitation beam  $\lambda_{\text{ex}}$ , (ii) the angle of incidence of the excitation beam  $\vartheta_1$  and (iii) the refractive indices of the two media  $n_1$  and  $n_2$ . The refractive index of a biological sample is out of our control and that of the first medium cannot be changed during the experiment. Moreover, available fluorophores require a specific excitation wavelength. Therefore, researchers control the penetration depth by varying the angle of incidence of the laser light until they find a good compromise in image quality. Figure 1.13 shows the ray path and the filtering scheme inside the microscope.

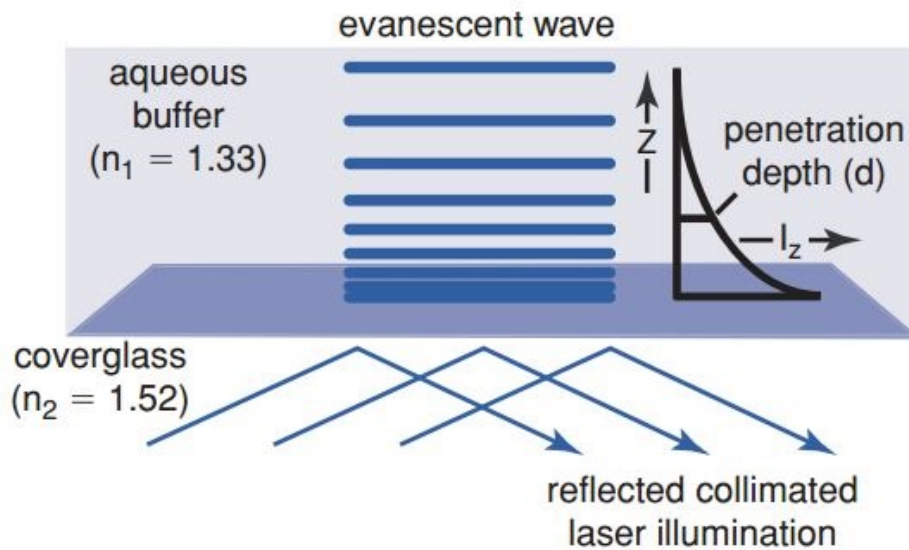


**Figure 1.12:** The evanescent wave and the penetration depth. In total internal reflection, an evanescent wave penetrates into the second medium for about 100 nm counting perpendicularly to the interface. Within this distance the fluorophores present in the sample can be excited. Image taken from [41].

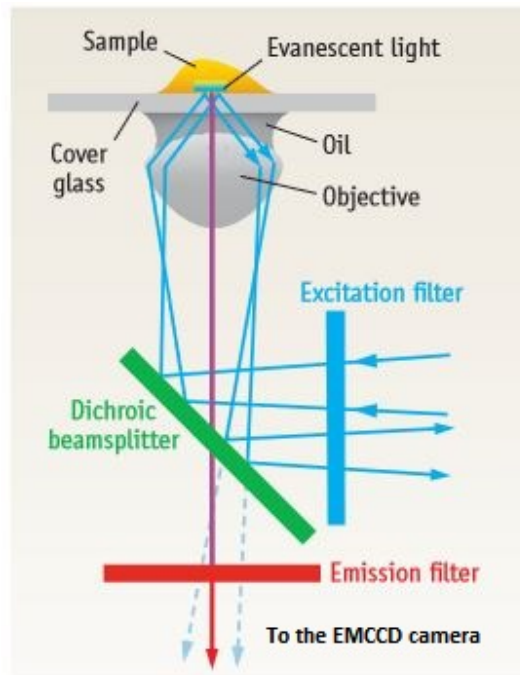


**Figure 1.13:** Ray path and the filtering scheme inside the microscope adjustable for reaching TIR. Image adapted from [38].

To sum up, total internal reflection fluorescence microscopy (TIRF) is a high signal-to-noise ratio technique that can be used to obtain a very thin optical section of a specimen whilst minimising background noise [42]. As depicted in Figure 1.14, it exploits the unique properties of an evanescent wave created in a limited region of the specimen that is adjacent to the interface between two media of different refractive indices, usually the aqueous specimen and the glass coverslip. In the present work, an oil immersion objective was used having the characteristic of a refractive index equal to that of the glass such that the only interface is the glass-specimen one.

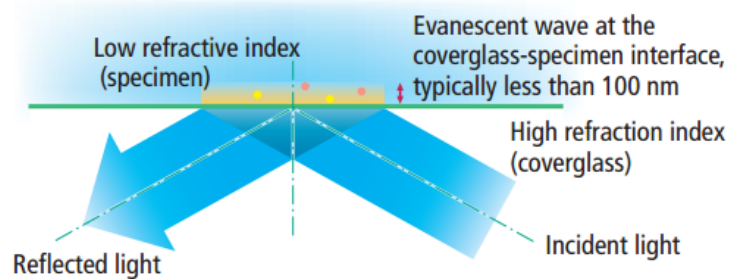


**Figure 1.14:** Creation of an evanescent wave at the coverglass-specimen interface capable of exciting the fluorophores inside the sample for some 100 nm counting the distance perpendicularly to the interface. Image taken from [43].

## 1.5 Organisation of this work

Chapter 2 describes chemical preparation methods and image processing algorithms from an operative point of view.

Chapter 3 illustrates the findings of this activity giving possible explanations to the facts observed.

Chapter 4 summarises the findings shortly offering some ideas valid as a guidelines for better quality experiments reducing the impact of the pitfalls of the "tools".

The experiments were conducted preparing a supported lipid bilayer with the three proteins mentioned earlier for image recording with a TIRF microscopy. Next, image processing stages yielded brightness of each protein and estimate the relative diffusion coefficient.

## Chapter 2

# Materials and Methods

---

The present chapter offers a brief coverage of the 'tools' that made the whole work possible pointing out how the single pieces work in a synergic fashion towards the final outcome. To begin, the structure and production steps of the protein probes used for the research will be presented. The chemical part continues with the protocol followed to create a supported lipid bilayer to which the proteins are finally attached. The third section deals with the microscope system used. Finally, the last section presents in a concise way the series of computer programmes utilised for the data analysis carried out in Matlab®.

### 2.1 The protein probes utilised

The protein stocks utilised to conduct the experiments described in this research master's thesis have been prepared for this purpose by our collaborator Dr. René Platzer from the Center for Pathophysiology, Infectiology and Immunology at the Institute for Hygiene and Applied Immunology of the Medical University of Vienna.

Streptavidin is an 56-kDa homotetramer from the bacterium *Streptomyces avidinii* that binds up to four biotin molecules [46]. The protein streptavidin and its small ligand biotin exhibit an extremely high binding affinity and specificity [47]. Figure 2.1 depicts the chemical structure of biotin and a pictorial representation of streptavidin with its four subunits, each presenting a site for binding a biotin molecule.

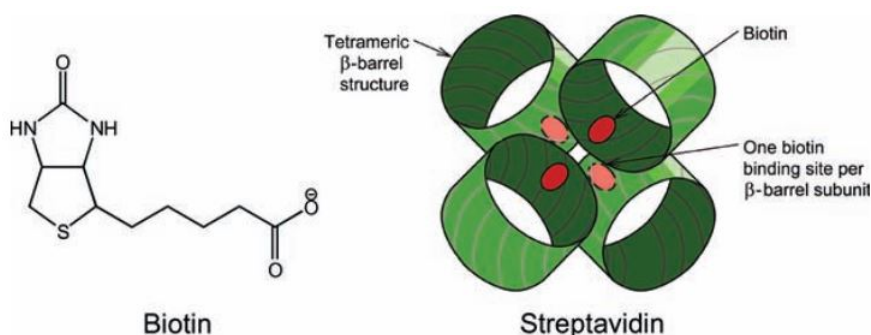


**Figure 2.1:** Chemical structure of biotin and a sketch of the streptavidin tetramer highlighting the binding site for biotin in each subunit. Image taken from [47]

Full details about the production protocol of the mSav platform (A106C, 3x6Histag) can be found in the methods section of a paper published by Dr. Rene Platzer [22] to which the reader is referred. However, it is important for a better understanding of the thesis's content, to briefly explain the production protocol also in this thesis, without any claim for exhaustiveness since it is beyond the scope of this investigation to dig into aspects in the field of bioanalytical chemistry too much.

For the present research, monovalent streptavidin was desired. Two monovalent versions of streptavidin were made, which differ in the chemistry applied to conjugate a single Alexa Fluor 647 (AF647) fluorophore to the protein. The final results were a monovalent Streptavidin with the dye linked site-specifically to a cysteine residue (mSav-C-AF647) via maleimide chemistry, and a monovalent Streptavidin where the dye was conjugated site-specifically to biotin (mSav-B-AF647) via NHS functionalisation. Both mSav versions carry 3x6 Histidine tags. Figure 2.2 shows the chemical structures of the AF647 fluorophore in the two cases. The tiny difference resides only in how the bottom chain on the left-side binds to the rest.



(a) Chemical structure of AF647 dye with Maleimide functionalisation (b) Chemical structure of AF647 dye with NHS Ester functionalisation

**Figure 2.2:** The two functionalisation methods used during production of protein probes. Images taken from fluoroprobes.com

To arrive at mSAv\*-3xHis6, only one subunit of the streptavidin was kept as biotin-binding and hence, termed alive (see Figure 2.3). In contrast, the other three subunits were made non-binding, termed dead. The C-terminus was equipped with a 6x histidine tag (His6) for attachment to a lipid bilayers containing DGS-NTA(Ni).

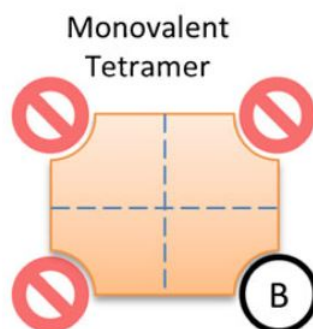


**Figure 2.3:** Sketch of the streptavidin tetramer with only one active subunit yielding a monovalent streptavidin (mSAv) with one binding site B. Image taken from [46]

In order to obtain a monovalent streptavidin that could be conjugated in a site-specific fashion to maleimide-functionalised fluorescent AF647 dyes, the binding subunit was modified by substituting an alanine for a cysteine residue at position 106 (A106C) as shown in Figure 2.4. To sum up, a monovalent streptavidin with cysteine linked to the Alexa Fluor 647 dye has been produced so far through maleimide chemistry.

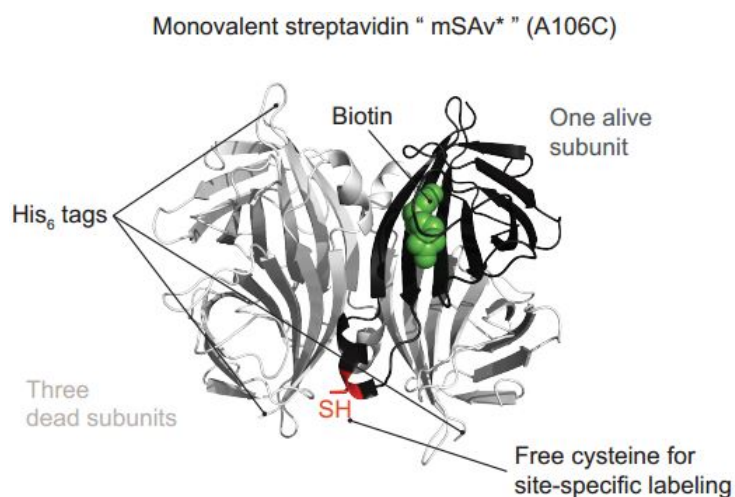


**Figure 2.4:** Crystal structure of monovalent streptavidin. Positions for molecular modifications to anchor photoactivatable organic dyes Alexa Fluor 647. Image taken from [22]

The monovalent Streptavidin with biotin (mSav-B-AF647), again with 3x6Histidine tags, has been made by mean of the same mSav platform described above without a free cysteine. In this mSav version, NHS chemistry links the same AF647 dye to biotin. A sketch of the geometry with the AF647 fluorophore and the Histidine tags can be seen in Figure 2.5.

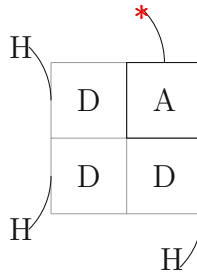


**Figure 2.5:** Sketch of the monovalent Streptavidin with the fluorophore AF647 attached to the alive subunit A (capable of binding biotin) and the three Histidine tags H on the dead subunits D (unable to bind biotin)

A good fluorescent molecule has several requirements to fulfil [47] and must be carefully chosen in the experiment planning phase [48], [49]. Among those requirements, a high photostability is essential to assure re-excitability a number of times before photochemical degradation occurs. The Alexa Fluor 647 dye chosen for this investigation is of common use in the scientific community nowadays.

As a third probe, a Major Histocompatibility Complex (MHC) class II protein loaded with an Alexa Fluor 647 labelled peptide linked through maleimide chemistry was also used, its crystal structure with the peptide in yellow is shown in Figure 2.6. An overview about the production protocol of pMHC can be found, for example, in [23] or [24].

For the present work, it is sufficient to draw the reader's attention on the fact that this pMHC probe has only two histidine tags (2xHis6), in contrast to the monovalent streptavidin probes, which have three each. As a consequence, the pMHC will be less strongly bound to nickel ions present in the bilayer.

Since the Ni-NTA was intentionally inserted in the SLB mixed with POPC lipids and the three protein probes come equipped with His-tags, it follows that the protein probes will anchor to the bilayer via affinity interaction between Nickel ions and His-tags [15]. For completeness, the actual process of equipping a protein with His-tags in the first place is done via a number of chromatographic stages which exploration go far beyond the scope of this thesis. The interested reader is referred to specialised literature like [16], [17].

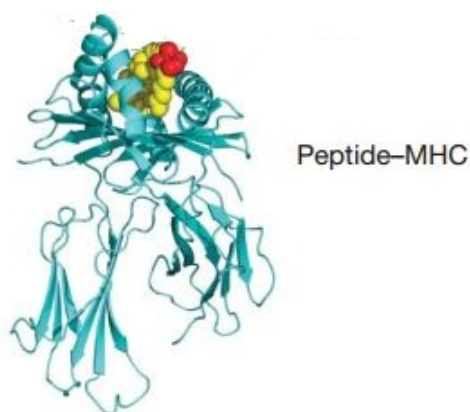


**Figure 2.6:** crystal structure of Peptide-MHC. The peptide has a cysteine residue (not visible here) to anchor, site-specifically via maleimide chemistry, a photoactivatable organic Alexa Fluor 647 dye. Image taken from [23]

## 2.2 Preparation of Supported Lipid Bilayers

Supported lipid bilayers (SLBs) enjoy great popularity among scientists in chemistry, biology, material science and several biomedical fields [27] as an easy-to-make mimic of the cell membrane on solid surfaces as in Figure 2.7.

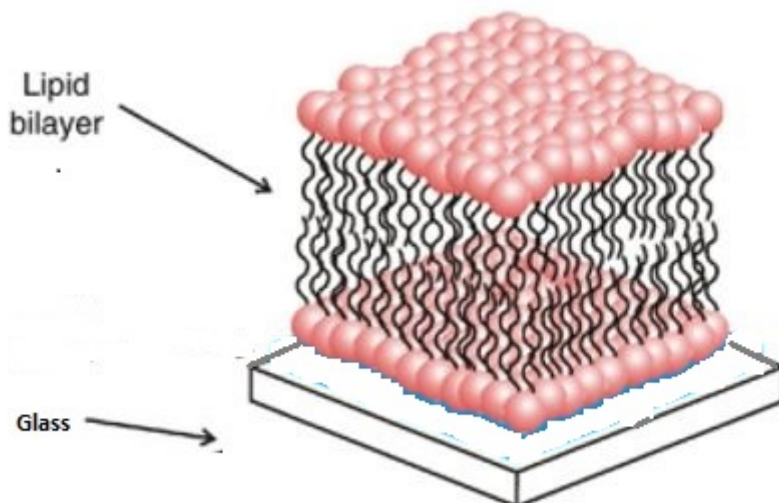


**Figure 2.7:** 3D Sketch of a supported lipid bilayer. Image adapted from [27]

### 2.2.1 Lipid vesicles preparation

A 10 mg stock of 1-palmitoyl-2-oleoyl-glycero-3-phosphocholine (POPC) in powder form was purchased from Avanti Polar Lipids and dissolved in 1 ml of chloroform for use. In addition, a stock solution of DOGS (Ni-NTA) at concentration (C) 1 mg/ml, purchased again from Avanti Polar Lipids, was also taken from available laboratory stock material. In order to allow for the subsequent binding of the histidine-tagged proteins, a mixture of 98% POPC and 2% Ni-NTA was prepared under the hood following the standard laboratory protocol described below.

The target is to have 1 ml of a mixture of 98% POPC and 2% Ni-NTA with a final concentration of 125  $\mu\text{M}$ . Hence, a volume of 9,3  $\mu\text{l}$  of POPC stock solution (10 mg/ml) is pipetted into a Fiolax tube and immediately followed by 2,6  $\mu\text{l}$  of Ni-NTA stock solution (1 mg/ml). Chloroform is evaporated by using low pressure Nitrogen for 15 minutes. Next, 1 ml of 10x DPBS buffer solution is added and the tube sealed with parafilm after quick Nitrogen filling to replace air. The following step is vortexing in order to reach a milky suspension. This

milky suspension undergoes sonication in a water bath at room temperature for ten minutes resulting in a finally transparent solution meaning that the vesicles are correctly formed. During sonication, it is fundamental to stay away from the lipid transition temperature to assure mobile vesicles are formed. Details about lipid phase transitions can be found for instance in [51]. To guarantee stable high quality standards, the vesicles used in each experiments were freshly made on the same day or max 48 hours earlier and stored in the fridge at 4°C.

### 2.2.2 Creation of a SLB on a glass surface

A glass slide is made temporarily hydrophilic via plasma cleaning and glued to a Labtek chamber using a dental glue (to ensure biocompatibility). Some details about the underneath biophysics can be found, for instance, in Rädler's article [32] and in Schönherr's article [30].

Finally, 200  $\mu\text{l}$  of the prepared vesicle mixture is added to each well. The Labtek chamber is covered with aluminium foil for 15 minutes of incubation to allow the bilayer to actually form onto the glass. Each well is then rinsed with about 25ml of 1xDPBS and the meniscus is removed. As a last step, 330  $\mu\text{l}$  of 1xDPBS is removed from each well.

### 2.2.3 Preparation of the proteins to be added to the SLB

All proteins used in the work were already coupled with the red dye Alexa Fluor 647 as described at the beginning of this chapter. Protein preparation for each experiment is carried out by diluting as desired a previously calculated amount of protein taken from the frozen stocks received from our collaboration partner Dr. René Platzer <sup>1</sup>. The stock solutions available are reported in Table 2.1.

**Table 2.1:** The stock solutions used for the experiments.

Protein Stock	Stock Concentration [ng/ $\mu\text{l}$ ]
mSav Biotin	160
mSav Cysteine	130
pMHC	71

<sup>1</sup>Center for Pathophysiology, Infectivology and Immunology at Institute for Hygiene and Applied Immunology of the Medical University of Vienna

Once ready, 50  $\mu\text{l}$  of diluted proteins in desired concentration (see Table 2.2) are added to the dedicated well in the Labtek chamber where the vesicles from the previous step have formed a SLB. Special care must be taken during this step to avoid creating any bubble in the well as it would destroy the SLB immediately.

**Table 2.2:** The final concentrations utilised for the experiments.

mSav Biotin [ng/ $\mu\text{l}$ ]	mSav Cysteine [ng/ $\mu\text{l}$ ]	pMHC [ng/ $\mu\text{l}$ ]
0,0030	0,0028	0,0071
0,0064	0,0065	0,0071

The Labtek chamber is stored in a Petri dish and covered with an Aluminium sheet to protect the fluorophores from light. Incubation time is 60 minutes. Each well is then rinsed with about 25ml of 1xDPBS and the meniscus removed. As a last step, 330  $\mu\text{l}$  of 1xDPBS is removed from each well. Table 2.3 presents the amount of protein inserted in each well in the two different dilutions steps utilised.

**Table 2.3:** Amount of protein present inside the 50  $\mu\text{l}$  of diluted solution pipetted in the well before incubation.

mSav Biotin [ng]	mSav Cysteine [ng]	pMHC [ng]
0,15	0,14	0,35
0,32	0,32	0,35

## 2.3 Microscope system, laser and camera

An inverted light microscope Zeiss Axiovert 200 with an oil immersion objective ( $\alpha$ -plan-Apochromat 100x/1.46 oil DIC (UV) VIS-IR) is used in TIRF configuration in combination with an Oxixus Simply Light laser source. The laser pulses are directed through the objective under TIRF conditions onto the fluorophores present in the lipid bilayer from the bottom of the sample. The same objective collects both reflected light and fluorescent light. A dichroic mirror set FITC/Cy5T (manufacturer Chroma, code zt488/640rpc) separates the two light components and a single band pass filter for the 647 nm wavelength (manufacturer Semrock) isolates the fluorescent part for detection via an Andor

EMCCD camera. All these steps are controlled by the dedicated software written in Labview on the computer system connected to the microscope, which provides calibration of the TIRF angle, the laser beam controls and the EMCCD camera settings. Table 2.4 below lists some of the chosen parameters.

**Table 2.4:** Important settings chosen for the experiments in Sequence mode as part of the Lab-view interface available at the microscope.

Important Settings chosen	
Time illum. [ms]	5
Time delay [ms]	20
Nmacro	35
Gain	300

### 2.3.1 Laser power settings

The necessity to avoid bleaching for preservation of the original SLB surface density and brightness as long as possible, led to select the power settings reported in Table 4.1. Special care has to be taken in choosing always very similar values and limiting fluctuations to minimise unavoidable environmental variations in room temperature and humidity. The laser power was measured each day with the same powermeter device about an hour before the actual measurements took place.

**Table 2.5:** The laser powers chosen for the experiments.

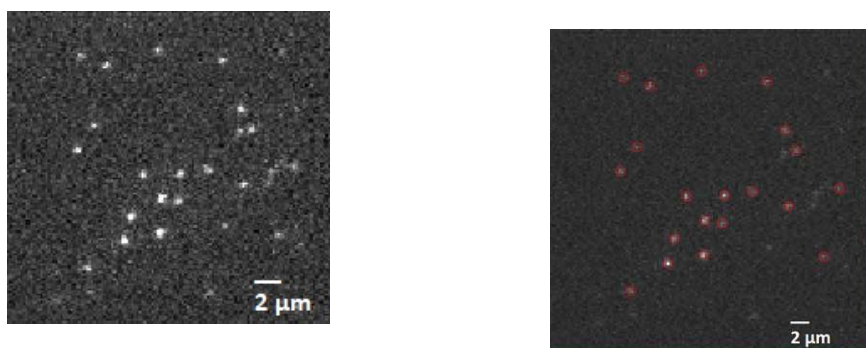
Laser Power settings	Focusing Power [kW/cm <sup>2</sup> ]	Imaging Power [kW/cm <sup>2</sup> ]
Low	0,16	0,16
High	0,16	0,24

## 2.4 Data analysis with Matlab and Fiji

The starting point is a visual inspection of the measurements carried out with Fiji to assure suitable quality level for the subsequent data analysis in Matlab, to be performed via in-house developed programmes available to the whole Biophysics Group.

### 2.4.1 Identification of the single molecule signals

A critical aspect is the definition of a threshold in brightness to count a diffraction limited spot in the image as a single molecule signal. This value is chosen by experience and testing each day by inspection of some of the molecules detected in the first image of few measurements. The same threshold applies for all the measurements performed on the same day. Detection is carried out through the program `prepare_peakposition` which localises the signals (see Figure 2.8) and fits them with a Gaussian function to obtain the xy-position, standard deviation, brightness and background of each signal and stores the result in dedicated files. Next, a second program called `check_fit` allows visual selection of a Region of Interest (ROI) per file generating a correspondent `pks` files. To assure consistency, the same ROI was applied to all files recorded on the same day using a specific feature of the program. Furthermore, through the functions `filter_pks` and the following `plot_pdf`, it is possible to plot normalized probability density functions (pdf) of brightness values. The pdf is calculated as normalized sum of Gaussians, in which the mean equals the detected brightness and the standard deviation equals the square root of the detected brightness multiplied by an appropriate smoothing factor used for all individual single-molecule signals.

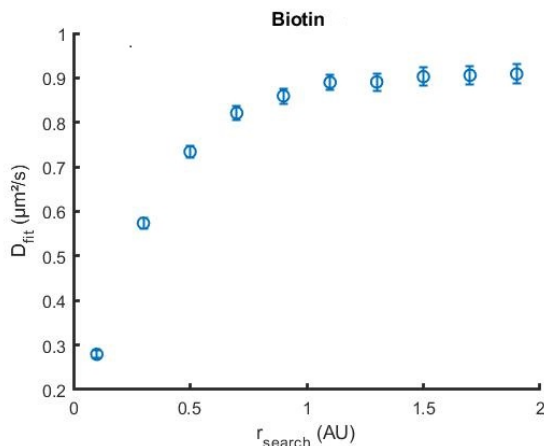


(a) A Supported lipid bilayer showing the single-molecule signals as originally recorded by the microscope's camera. (b) The red circles indicate the single-molecule signals detected after the application of `prepare_peakposition`.

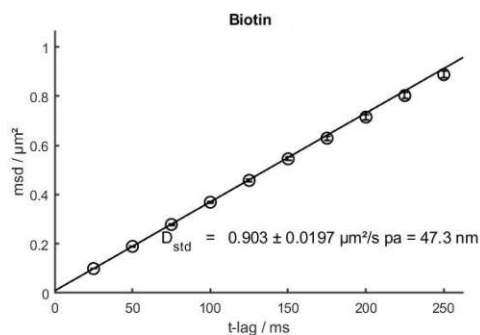
**Figure 2.8:** These pictures illustrate the same SLB before and after the application of the detection algorithm.

## 2.4.2 Estimation of the diffusion coefficient for the three probes.

A parameter of great importance when dealing with proteins or lipids in mobile lipid bilayers is the diffusion coefficient. A suitable method for calculating it, is through Single Particle Tracking, as Rose et al. point out [52]. Further details about the potential of the Single Particle Tracking approach can be found in [54]. Let's now focus our attention on how it was utilised in the thesis. The diffusion coefficient's estimation was performed via the two functions written in Matlab named `auto_catch` and `msdplot` which have been already in use at the Biophysics group for years. The function `auto_catch` takes as input the pks files introduced in the previous paragraph, and uses them to track the single molecules detected by `prepare_peakposition` along the subsequent frames. The tracking is based on searching for the single molecule's position within a certain distance, frame after frame. This quest is executed for several increasing radii in a range specified by the user. The data are stored in a matrix reporting, for each single molecule's signal, in which frame the molecule was detected and up to which subsequent frame this very same signal was still encountered and the position occupied in each frame. Next, a plot is generated from these data showing the calculated diffusion coefficient for each search radius. Finally, the saturation radius is chosen by the user based on the inspection of the plot. Figure 2.9a shows a sample plot where the value  $r_s = 1,5$  identifies the onset of the saturation regime. The tracking data related to this radius are now elaborated via the Matlab function `msdplot` which yields the numerical estimation of the diffusion coefficient with its error, as depict in Figure 2.9b. In order to assure for dataset comparability, the saturation radius was kept the same for all the data sets recorded on the same day. This means that the saturation radius has to be chosen appropriately to be valid for all datasets.



(a) Saturation curve for selecting the search radius  $r_{\text{search}} = 1,5$  for the subsequent estimation of the diffusion coefficient.



(b) The fitting for the chosen radius of saturation  $r_{\text{search}} = 1,5$  yields the Diffusion coefficient with its error

**Figure 2.9:** Sample plots of the Diffusion Coefficient estimated via Matlab for the Biotin sample recorded in high laser power.

### 2.4.3 Surface Density estimation

The parameter of single molecule's surface density in units of molecules/ $\mu\text{m}^2$  can be heavily affected by photobleaching. Therefore, only the first image of each measurement has been considered in the calculation. In fact, the very first image is the one which has being exposed to the least bleaching effect.

A visual inspection of the measurements with the three proteins using Fiji yielded that the probes were present at low densities on the SLB. This kind of bilayers require a specific approach for their surface density determination. For this purpose, a matlab function called `get_low_densities` was adapted from a previous research activity by Bishara [53] carried out at the Biophysics Group. The pks files generated earlier through the function `check_fit`, are given as input for the function and yield the mean value and the deviation from the mean (SEM) of the surface density in the ROI for each file. This is achieved by counting the number of identified single-molecule's signals in every first image

and dividing them by the ROI area expressed in  $\mu\text{m}^2$ . Then, the overall mean and SEM over the whole data set is calculated. In conclusion, the values obtained for the surface density of the three protein samples are listed in Table 2.6 Note that pMHC column reproduced twice for the sake of symmetry is the same on both tables because it was exactly the same physical well.

**Table 2.6:** Surface density for the three probes. The amount of protein added into the well is reported next to the probe's name. All experiments were performed on the same day.

ROI	Imaging Power [kW/cm <sup>2</sup> ]	mSav Biotin 0,15 ng [molecules/ $\mu\text{m}^2$ ]	mSav Biotin 0,32 ng [molecules/ $\mu\text{m}^2$ ]	pMHC 0,35 ng [molecules/ $\mu\text{m}^2$ ]
Small ROI	Low 0,16	0,1019 $\pm$ 0,0058	0,1435 $\pm$ 0,0081	0,2759 $\pm$ 0,0073
	High 0,24	0,0878 $\pm$ 0,0057	0,1520 $\pm$ 0,0110	0,2943 $\pm$ 0,0079
Big ROI	Low 0,16	0,4100 $\pm$ 0,0125	0,5757 $\pm$ 0,0273	0,1260 $\pm$ 0,0022
	High 0,24	0,3742 $\pm$ 0,0107	0,7780 $\pm$ 0,0394	0,1560 $\pm$ 0,0034
ROI	Imaging Power [kW/cm <sup>2</sup> ]	mSav Cysteine 0,14 ng [molecules/ $\mu\text{m}^2$ ]	mSav Cysteine 0,32 ng [molecules/ $\mu\text{m}^2$ ]	pMHC 0,35 ng [molecules/ $\mu\text{m}^2$ ]
Small ROI	Low 0,16	0,0413 $\pm$ 0,0036	0,0440 $\pm$ 0,0033	0,2759 $\pm$ 0,0073
	High 0,24	0,0438 $\pm$ 0,0036	0,0480 $\pm$ 0,0040	0,2943 $\pm$ 0,0079
Big ROI	Low 0,16	0,1205 $\pm$ 0,0081	0,1378 $\pm$ 0,0067	0,1260 $\pm$ 0,0022
	High 0,24	0,1422 $\pm$ 0,0064	0,1684 $\pm$ 0,0066	0,1560 $\pm$ 0,0034



Die approbierte gedruckte Originalversion dieser Diplomarbeit ist an der TU Wien Bibliothek verfügbar  
The approved original version of this thesis is available in print at TU Wien Bibliothek.

## Chapter 3

# Results

---

The present chapter covers the findings of the experimental activity where supported lipid bilayers of three protein probes - a pMHC and two versions of monovalent streptavidin in which the dye is linked via a biotin or a cysteine residue - were produced as illustrated in detail in the previous chapter. They were measured via TIRFM and analysed via specific image processing algorithms (see again Chapter two for details). The aim of the experiments has been two-fold: (i) to investigate if and how some standard chemical binding methods used to link a fluorescent dye to the protein can influence a monomer's brightness. (ii) to determine optimal imaging conditions for recording a reliable monomer brightness distribution. The reason behind the choice of monomeric samples lies in their intrinsic feature of being single-molecule candidates by default. This is a fundamental characteristic to use them later as single-molecule reference in order to assess brightness correctly. Hence, the brightness distributions obtained for the probes will be presented. To follow, several graphics support to develop a possible explanation for the observed behaviour. The fourth section deals with estimating the diffusion coefficient of each probe and contextualises it elucidating the response of the probes to laser-induced brightness distribution. In conclusion, a bird's eye view on the main aspects discussed in the chapter is given in a very concise way to emphasise, once more, the optimal settings for conducting brightness based experiments.

### 3.1 Some important chemical remarks

Cysteine is one of the two sulphur-carrying amino acids (see Figure 3.1) that acts as a building block of proteins. Maleimide–thiol coupling (Figure 3.2) is a common choice in the scientific community today for the chemical modification of proteins through cysteine residues [18]. This method allows linking a fluorophore, e.g. the AF647 used in this work, to a cysteine in a site-specific fashion. Two protein probes out of three were prepared using this technique: a monovalent streptavidin labelled on an unpaired cysteine (A106C) with maleimide-AF647 (mSav-C-AF647) and a pMHC class II molecule site-specifically labelled with maleimide-functionalised AF647 linked to the peptide. The third protein was another version of monovalent Streptavidin where an NHS-functionalised AF647 dye was conjugated to a biocytin (biotin-lysine complex) linked to the streptavidin (mSav-B-AF647). Briefly, here an NHS ester reagent couples to the  $\alpha$ -amine at the N-terminal end and the  $\epsilon$ -amines of lysine side chains [21] of the biocytin. The three probes are also equipped with Histidine tags to bind through Nickel ions to the lipid bilayer.

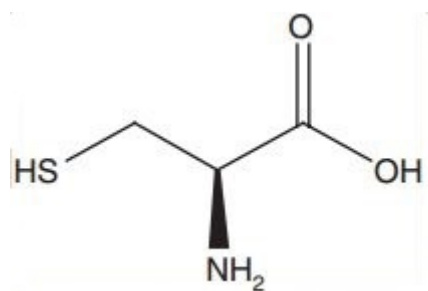


**Figure 3.1:** The chemical structure of the sulfur-carrying amino acid cysteine. Image taken from [16]

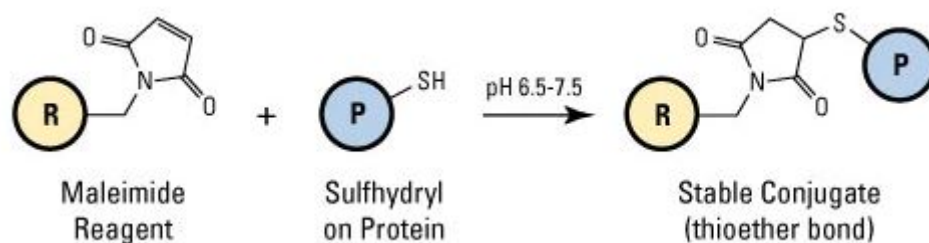
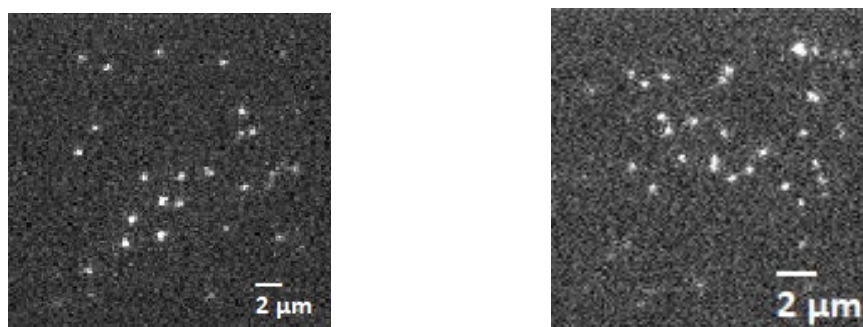


**Figure 3.2:** Scheme of cysteine-mediated protein modification via maleimide. The R ball indicates the AF647 fluorophore linked to a maleimide group, while the P linked to sulfhydryl -SH group indicates the protein bound to a cysteine. Image taken from [19]

## 3.2 Brightness distributions

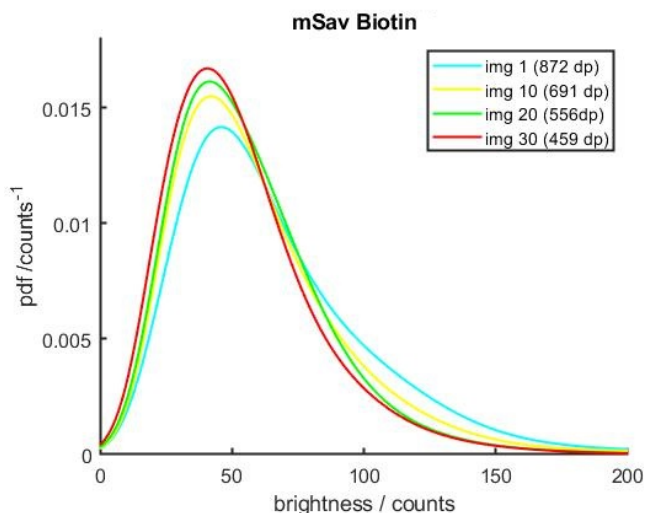
After preparing lipid bilayers as described in Chapter 2 with the proteins anchored to them via histidine tags-nickel ions interactions, see the previous chapter for details, fluorescence microscopy took over. To follow, the analysis of imaging data of these supported bilayers as those illustrated in Figure 3.3 performed in Matlab via in-house developed programmes available to the whole Biophysics Group.



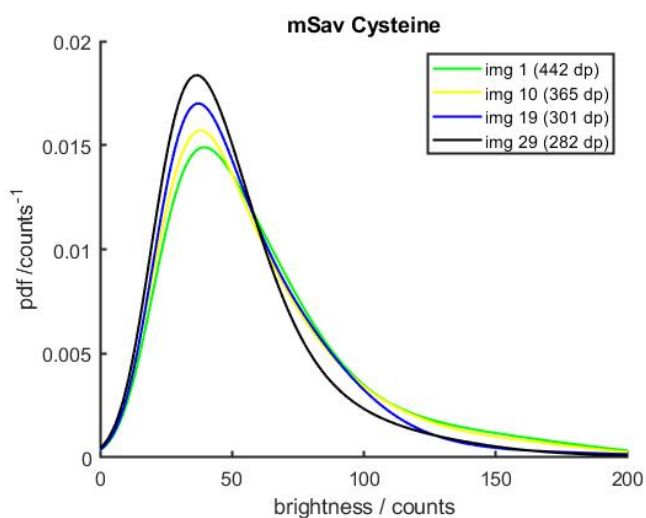
(a) A Supported lipid bilayer of the biotin sample showing the single-molecule signals as originally recorded by the microscope's camera. (b) A Supported lipid bilayer of the pMHC sample showing the single-molecule signals as originally recorded by the microscope's camera.

**Figure 3.3:** These pictures illustrate some SLB as recorded by the fluorescence microscope.

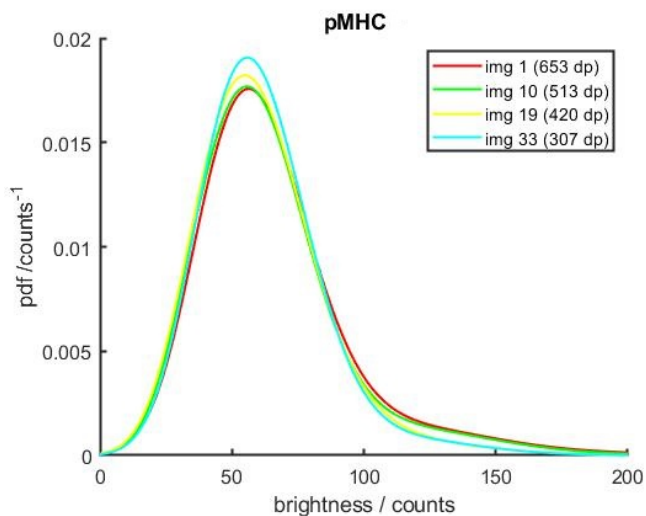
These algorithms identify the single molecule's signal in every frame present in each dataset based on a preset brightness threshold, for details about the algorithm functioning see the dedicated section in Chapter 2. The next step is to generate a probability density function displaying the brightness distribution per frame in a plot. Figure 3.4 shows an example of such plots of the brightness distribution for the two streptavidin probes and the pMHC probe. These probability density functions for the three probes were created with the same analysis settings from samples measured on the same day under identical imaging conditions. The curves displayed were calculated for increasing frame numbers to present an overview over the time course of an experiment. Note that the brightness values used to generate one curve originate from several imaging files. All graphs illustrate a peak's shift to the left side towards lower brightness values that becomes more pronounced as the measurement progresses. A closer look at Figure 3.4 tells that this effect appears to be a function of the image number and also that it is present to a different extent depending on the probe considered. The biotin probe shows the most pronounced shift, while the shift seems almost absent for pMHC.



(a) Brightness distribution of the biotin probe at high imaging power.



(b) Brightness distribution of the cysteine probe at high imaging power.



(c) Brightness distribution of the pMHC probe at high imaging power.

**Figure 3.4:** Plot of the probability density functions for the three probes illustrating a peak's shift to the left side towards lower brightness values as the measurement progresses. This effect is present to a different extent in all probes, with Biotin showing it the most and pMHC the least. The legend says the available data points per image.

The visual inspection of the recorded images with the programme Fiji indicated for these low-density SLB the absence of overlapping signals that could have been considered responsible for the observed phenomenon by causing detection errors by the fitting algorithms. In fact, two overlapping signals can be easily regarded as one molecule which would give an erroneous higher brightness value, which, decreases with the duration of the experiment because one of the two molecules will bleach during laser light exposure.

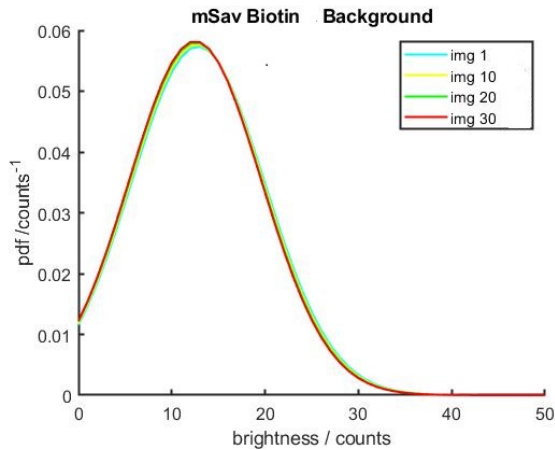
A proof to exclude a significant presence of overlapping signals in the images is given by the local background of individual fitted signals. As a matter of fact, given two molecules close to each other, the local background would be the same if both signals overlap within the resolution limit. However, when the density is too high for accurate fitting, then signals too close to one another would yield an increased background for the fitted one. In other words, let's say the fitting window is 7x7 pixels, so if the next signal is closer than e.g. 4 pixels, some photons of it will contribute to the background of the fitted signal.

A possible way to verify the local background of individual fitted signals is by generating the same probability density functions of Figure 3.4 but considering local background brightness values instead. Examples of such plots can be seen in Figure 3.5a for biotin. This control pointed out that the local background brightness for every molecule is constant over all frames, in contrast to the brightness distribution observed for the single-molecule signals. In addition, a preliminary control performed on the camera background/offset assures that it is constant during the measurement.

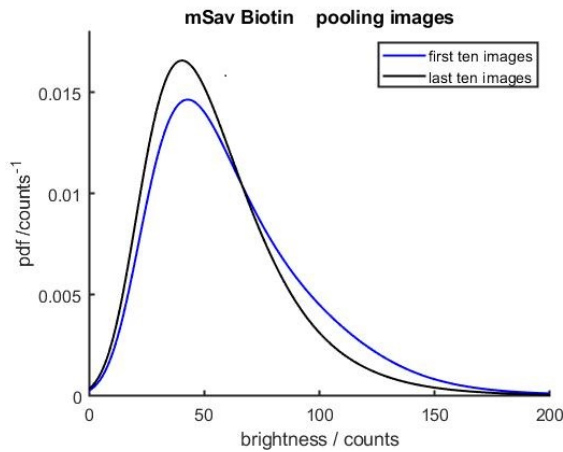
### 3.3 Pooling of images for better visibility.

The shift of brightness towards lower values with increasing frame number is sometimes hard to observe in pdf plots as those reported in Figure 3.4. To overcome this, a dedicated Matlab function pooled the images. Such a function generates a brightness distribution plot where a group of images are combined to improve statistics for better visualisation concerning the number of data points given for each coloured curve in Figure 3.4. This simple solution remarkably improves the visual clarity of the presented data and will be the author's choice to comment on the three proteins' behaviour from now on.

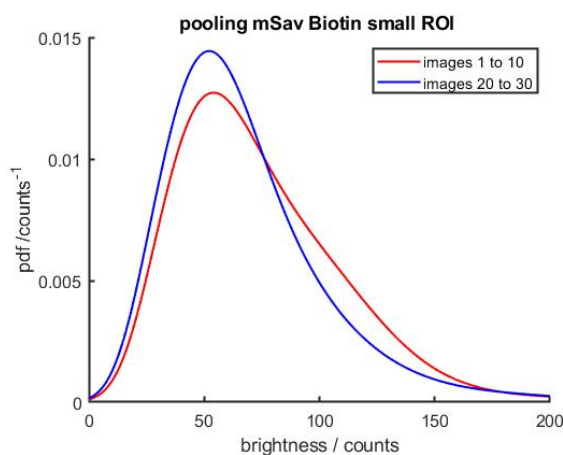
Figure 3.5b presents the pooling of images taken from the same biotin data set considered in the preceding paragraph, differing only by the size of the Region



(a) Brightness distribution of the background of the biotin probe shown in Figure 3.4a. The curve shows only a very slight shift.



(b) Pooling for a large ROI of the first ten images and last ten images indicates a variation in Brightness between the beginning and the end of the experiment.

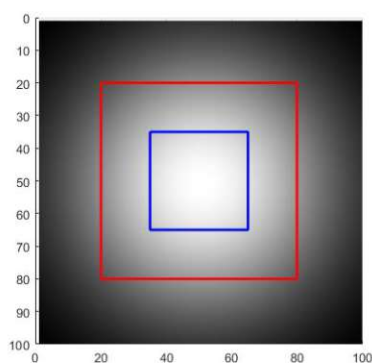


(c) Pooling for a small ROI of the first ten images and last ten images indicates a variation in Brightness between the beginning and the end of the experiment.

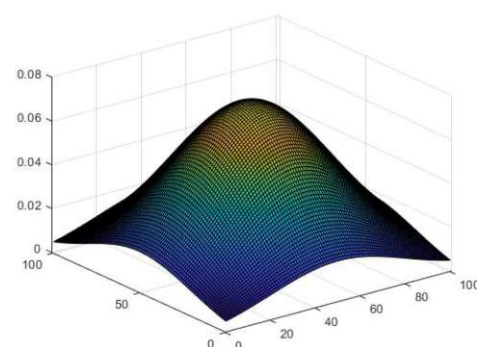
**Figure 3.5:** (a) Example of local background for the biotin probe. The pooled plots of the probability density functions for big ROI (b) and for small ROI (c). The peak's shift towards lower brightness values observed as the measurement progresses is present independently of the chosen ROI.

of Interest (ROI) considered in subplots b and c. The plots reveal, once again, that there has been a gradual drop in brightness over the experiment. Focusing our attention for a moment on Figure 3.5b, the black curve, i.e. data pooled from the last ten images, shifts to the left side towards lower brightness values with respect to the blue curve, i.e. data pooled from the first ten images. Similar conclusions can be drawn from 3.5c where only the ROI size was changed.

A hypothesis to explain the observed drop in brightness for higher frame numbers could be that, the single molecule's brightness in the centre of the ROI differs from the brightness at the edge. The basis for such a hypothesis lies in the fact that the laser intensity profile used here is a Gaussian one (see Figure 3.6 for a sketch of the situation). In laser systems, the bell shape yields a higher intensity in the centre, leading to more pronounced bleaching there.



(a) The blue and the red square represent small and big ROI respectively. The picture shows the portion of Gaussian laser profile interested by each ROI.



(b) 3D Plot of a Gaussian laser profile, the laser intensity depends on the position considered.

**Figure 3.6:** The Gaussian laser profile and how the laser intensity is affected by the chosen ROI. The light intensity is stronger within the small ROI, as the high brightness level inside the blue square in (a) depicts. This corresponds to the peak in the 3D plot in (b). Within the red square, i.e. the big ROI, gradual shades of grey are visible as the distance from the centre increases and laser intensity decreases.

It is worth to remark that the effect described is independent of the ROI. One proof of this independence is provided by the comparison of the mean brightness values in Table 3.1 calculated from data used to generate the pooled curves in Figure 3.5b-c for small and big ROI. These values point out that the brightness decreases in the same fashion for the three probes regardless of the ROI size. In fact, the difference between the late pool of images and the first pool for both ROIs yields similar values.

This indicates that the system's behaviour is not affected by the ROI selection. Worth noting in Table 3.1 is also that, again, the biotin's decrease in brightness is the strongest while pMHC shows the weakest, reaching roughly half the biotin's decrease.

**Table 3.1:** The average brightness for each probe is reported analysing the same data set in big ROI and in small ROI. The values obtained show numbers close enough to each other to consider the ROI size irrelevant. Note, however, that the brightness in small ROI has higher average values in comparison to the big ROI condition. as a natural consequence of the Gaussian profile of the laser.

Protein probe	pooled images	Average Brightness	
		Big ROI [counts]	Small ROI [counts]
pMHC	img 1 to 10	54,09	65,44
	img 20 to 30	50,17	62,45
Cysteine	img 1 to 10	60,51	69,64
	img 20 to 30	52,68	62,13
Biotin	img 1 to 10	63,76	75,68
	img 20 to 30	54,88	67,75

Furthermore, a closer look at the Table 3.1 reveals that the average brightness for the same pooled curves is always higher in the small ROI condition than in the big ROI case. In fact, the laser power per area for the small ROI is always higher which yields brighter molecules in that zone. This is why in small ROI the brightness distribution is shifted to higher values. Here is a first indication of the paramount importance of which region is observed in brightness experiments. A second proof will follow in the next paragraph where an analysis of the distance of single molecules from the centre of the ROI will be brought to the fore. Another crucial aspect is that, due to bleaching of the single-molecules by laser light, the number of molecules in later frames will always be lower.

Table 3.2 lists the percentage of bleached molecules over one experiment with the three proteins recorded under exactly the same experimental conditions. These percentages were obtained by counting the number of molecules detected in the ROI in the first ten pooled frames and in the last ten pooled frames.

By dividing the latter by the former, it was known the fraction of molecules remaining at the end of the measurement in percentage, and then the percentage of molecules bleached away was determined.

**Table 3.2:** The percentage of molecules lost due to bleaching from the onset to the end of an experiment for the three probes at equal imaging power and ROI on the same day.

Bleached molecules	
Protein	[%]
pMHC	33
Cysteine	27
Biotin	40

Additional data recorded to check whether reduced bleaching would help to preserve the single molecules for longer times turned out to be successful. By lowering the excitation power applied (see Table 3.3), single molecules lasted for more frames. To sum up, the same SLB was recorded at a lower imaging power and at high imaging power, while the focusing power was kept the same for both experiments. The remarkable result of this test is shown in Figure 3.7 which illustrates for a given ROI that lowering the applied imaging power reduces the shift towards lower brightness values. Hence, it is good practice to keep the imaging power as low as reasonably possible. In fact, by doing so, the single molecules will be bleached more slowly leading to stronger statistics in later frames, which yields more reliable results in the end.

**Table 3.3:** The laser powers chosen for the experiments.

Laser Power settings	Focusing Power [kW/cm <sup>2</sup> ]	Imaging Power [kW/cm <sup>2</sup> ]
Low	0,16	0,16
High	0,16	0,24

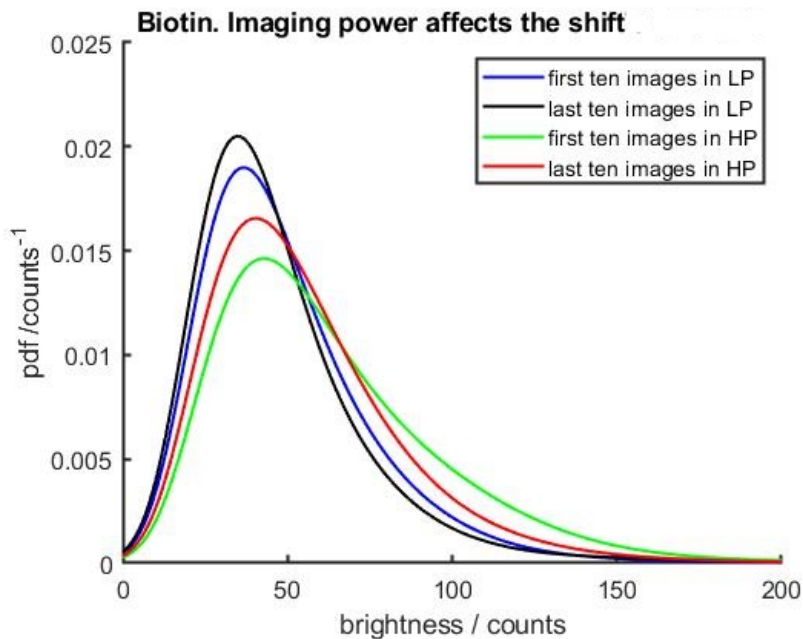
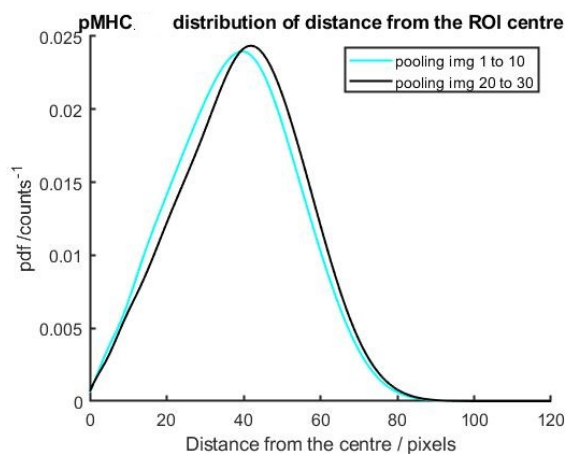


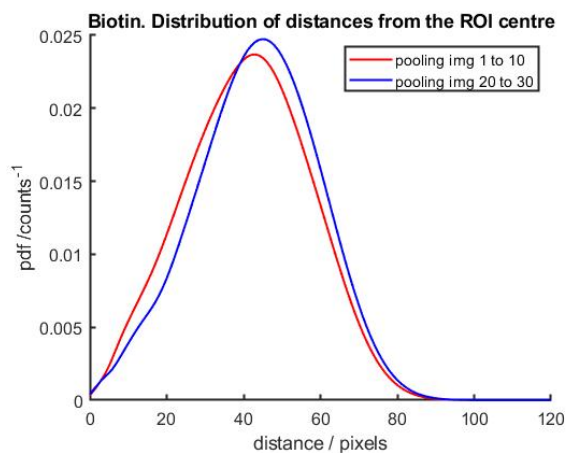
**Figure 3.7:** Comparison of pooled images recorded on the same SLB with different imaging powers and both analysed in large ROI. The shift in brightness between the beginning and the end of the experiment is more pronounced in the high power curves as expected.

### 3.4 How the distance from the centre affects the single molecule's brightness

So far, it has been argued that a decrease in the number of single-molecule signals is more pronounced in the central part of the ROI than at the edge. Figure 3.8 presents a distribution of distances from the centre for the molecules. A shift of the pooled curve representing the late frames towards the right-hand side is evident. This means that the number of molecules in the central part of the ROI decreases since the average distance of the molecules from the centre increases. This depopulation proves that the occurring loss of molecules is slightly more pronounced in the central region of the ROI.



(a) Plot of the average distance of the molecules from the centre of the ROI for the pMHC probe.

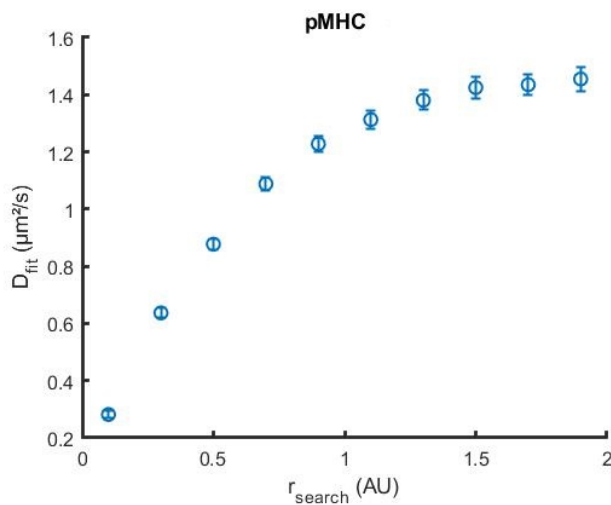


(b) Plot of the average distance of the molecules from the centre of the ROI for the biotin probe.

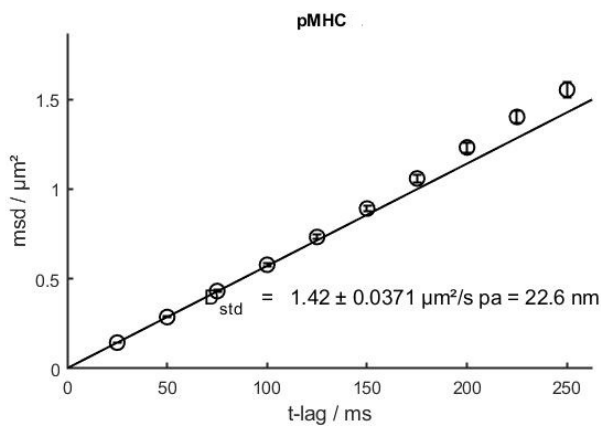
**Figure 3.8:** Pooling pdfs illustrating how the distance of the molecules from the centre of the ROI differs significantly from beginning to the end of the experiment. This proves that there are more molecules at the edge in later frames in comparison to earlier frames. A possible explanation is bleaching, since lower imaging power reduces the effect being, therefore, advisable experimental practice.

### 3.5 Estimation of the diffusion coefficient for the three probes

The diffusion coefficient of the proteins in each SLB was estimated via in-house Matlab programmes routinely used within the research group for this purpose. Figure 3.9 shows a sample plot for pMHC of how these programmes work, it is analogous to the plot presented for biotin in the previous chapter.



(a) Saturation curve for selecting the search radius  $r_{\text{search}} = 1,5$  for the subsequent estimation of the diffusion coefficient.



(b) The fitting of data for the chosen saturation radius  $r_{\text{search}} = 1,5$  yields the diffusion coefficient with its error

**Figure 3.9:** Diffusion coefficient estimated via Matlab for the pMHC sample with saturation radius  $r_{\text{search}} = 1,5$ .

To follow, Table 3.4 reports the values estimated by the msdplot fitting algorithm. Note that pMHC data is the same on both tables for better comparability.

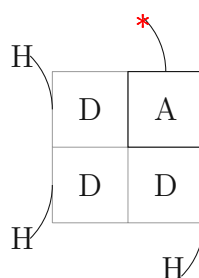
**Table 3.4:** The diffusion coefficient estimated for the three probes. The amount of protein added into the well in the experiment is reported next to the probe's name. All experiments presented were performed on the same day to enable a direct comparison.

Imaging Power [kW/cm <sup>2</sup> ]	mSav Biotin 0,15 ng [μm <sup>2</sup> /s]	mSav Biotin 0,32 ng [μm <sup>2</sup> /s]	pMHC 0,35 ng [μm <sup>2</sup> /s]
Low 0,16	0,882 ± 0,014	0,888 ± 0,018	1,35 ± 0,024
High 0,24	0,874 ± 0,016	0,903 ± 0,0020	1,42 ± 0,037

Imaging Power [kW/cm <sup>2</sup> ]	mSav Cysteine 0,14 ng [μm <sup>2</sup> /s]	mSav Cysteine 0,32 ng [μm <sup>2</sup> /s]	pMHC 0,35 ng [μm <sup>2</sup> /s]
Low 0,16	0,567 ± 0,022	0,678 ± 0,026	1,35 ± 0,024
High 0,24	0,757 ± 0,025	0,334 ± 0,019	1,42 ± 0,037

Among the three protein probes considered, pMHC exhibits the highest diffusion coefficient. An explanation for this could lie in the chemical features of the pMHC probe which has only two histidine tags to anchor it to the nickel ions present in the bilayer. In contrast, the mSav probes are both equipped with three histidine tags, i.e. one attached to each dead subunit of the streptavidin tetramer, as illustrates Figure 3.10.



**Figure 3.10:** Sketch of the monovalent Streptavidin with the fluorophore AF647 attached to the alive subunit A and the Histidine tags attached to the dead subunits D.

### 3.6 A look back at this chapter

To sum up, the results of this experimental activity pointed out the critical role that the imaging power plays in the outcome of brightness analysis experiments. In fact, the imaging power is the key parameter towards valid data gathering. As a rule of thumb, it should be kept as low as reasonably possible in order to avoid photobleaching. The presented data indicate that lower imaging power values preserve the single molecules in the central part of the ROI for longer times i.e. the lower is the imaging power applied, the lower will be the peak's shift (see Figure 3.7). Offering, therefore, more reliable brightness estimation in the end.

# Chapter 4

## Discussion

---

This chapter presents the take home message of the whole thesis.

### 4.1 What the experimental findings tell us

The findings of this experimental activity pointed out the critical role that the laser power plays when proper selection of image recording settings is of concern for the outcome of brightness analysis experiments. Photobleaching i.e. a loss of fluorescence intensity of the specimen caused by the interaction between the exciting light and the fluorescent compound [21], is a familiar issue to any experimenter doing fluorescence microscopy. Consequence of this process is the photochemical destruction of the fluorescent dye molecules, Alexa Fluor 647 in case of the present thesis. Since this loss of functional dyes occurs during the experiment, photobleaching affects to a large extent the collected images. This is the reason why later frames have less fluorescence signals detected by the fitting algorithm with respect to the first frames. However, an optimization of image recording parameters for the recording of several images in the quest of a good compromise, can greatly improve the situation leading to smaller differences in single-molecule signals recognised in frames taken at the beginning of the measurement and frames taken at the end. Figure 4.1 presents, as example, the same experimental data from the biotin sample recorded in the two imaging power conditions, low and high power (see Table 4.1), grouped in a single plot by means of the pooled curves introduced in the previous chapter. The shift between the pooled curves representing early and late stage of the experiment is much less in the low power case in comparison to the high power one. This indicates clearly that lower imaging power settings preserve the single-molecules

signals for longer times i.e. the lower is the imaging power applied, the more data points per frame will be detected.

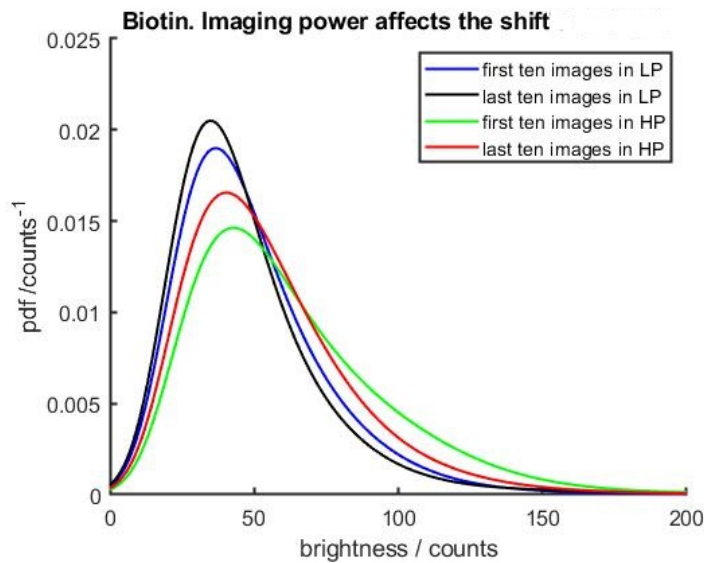


**Figure 4.1:** Comparison of pooled images recorded on the same SLB at different imaging powers. The shift in Brightness between the beginning and the end of the experiment is more pronounced in the high power curves as expected.

**Table 4.1:** The laser powers chosen for the experiments.

Laser Power settings	Focusing Power [kW/cm <sup>2</sup> ]	Imaging Power [kW/cm <sup>2</sup> ]
Low	0,16	0,16
High	0,16	0,24

A second aspect to be consider during preparation for brightness analysis experiments are the characteristics of the Gaussian laser profile. In fact, the observed drop in brightness for later frames can be ascribed to the different single-molecule's brightness in the centre of the ROI with respect to the brightness at the edge (see Figure 3.6). For laser beams, the bell-shaped profile yields a slightly higher intensity in the centre, leading to more pronounced bleaching there. Hence, choosing a small and well-centred ROI in the central zone of the laser beam offers more uniform intensity over the selected area.

## 4.2 Does diffusion play a role here?

Diffusion of single molecules has been studied by the scientific community already in some detail using several approaches, see for instance [54] and [55]. Tables 4.2 reports the diffusion coefficients estimated for the probes via the algorithms explained in Chapter 2. The values yielded by the algorithm in case of low laser power are close to those found for high laser power for Biotin and pMHC. This indicates that laser power does not affect the diffusional behaviour of the proteins. The values for the cysteine probe seem to be less close to one another. This is, in the writer's opinion, due to the poorer statistics available for this sample in the experiment presented in comparison to the other probes. Consequently leading the algorithm to not completely coherent estimations. For this reason, this apparent discrepancy should not cause any alarm here.

**Table 4.2:** The diffusion coefficient estimated for the three probes. The amount of protein added into the well in the experiment is reported next to the probe's name. All experiments presented were performed on the same day to enable a direct comparison.

Imaging Power [kW/cm <sup>2</sup> ]	mSav Biotin 0,15 ng [μm <sup>2</sup> /s]	mSav Biotin 0,32 ng [μm <sup>2</sup> /s]	pMHC 0,35 ng [μm <sup>2</sup> /s]
Low 0,16	0,882 ± 0,014	0,888 ± 0,018	1,35 ± 0,024
High 0,24	0,874 ± 0,016	0,903 ± 0,0020	1,42 ± 0,037
Imaging Power [kW/cm <sup>2</sup> ]	mSav Cysteine 0,14 ng [μm <sup>2</sup> /s]	mSav Cysteine 0,32 ng [μm <sup>2</sup> /s]	pMHC 0,35 ng [μm <sup>2</sup> /s]
Low 0,16	0,567 ± 0,022	0,678 ± 0,026	1,35 ± 0,024
High 0,24	0,757 ± 0,025	0,334 ± 0,019	1,42 ± 0,037

It is no doubt worth to spend some words in commenting the significantly higher diffusion coefficient of pMHC. This result could be specifically related to the structural aspects of the pMHC probe. Since the number of histidine tags differs between pMHC and the two monovalent streptavidin probes. The presence of only two His tags in pMHC, in contrast to the biotin and cysteine mSav samples, both of which are equipped with three Histidine tags. Therefore, pMHC can bind to less Ni-NTA-Lipids contained in the SLB. However, it was not possible to clarify if a less viscous drag takes place and the question remain open for further investigation.

## 4.3 Conclusions

As a rule of thumb, the imaging power should be kept as low as reasonably possible to reduce photobleaching of fluorescent molecules. In fact, the presented data indicate that lower imaging power values preserve the single-molecules in the central part of the ROI for longer times i.e. lower imaging power applied will yield a lower shift of the peak. Therefore, a careful choice of the laser power to be utilised should be the primary concern in any experiment involving brightness analysis, as it is a key factor in gathering useful data. A misleading or careless selection of too high imaging power could strongly alter the surface density estimation leading to incorrect scientific interpretations and conclusions. In fact, high laser power bleaches fluorescent single-molecule signals quicker plummeting statistics after the early frames very fast, poor statistics in image collection makes conclusions prone to errors.

For the analysis of a sample of unknown stoichiometry, the monomer signal from a reference experiment should be taken exactly from the same images i.e. the same frame numbers, and just from the beginning of the recording to investigated. Only then the estimation is correct.

Another aspect worth further verifications, which was not possible to clarify with the available data, is whether the differences observed in the brightness distribution among the probes of biotin and pMHC is caused by surface density related effects only, or the different chemical environments of the probes play also a role here.

# Bibliography

---

- [1] Mund M, Ries J. How good are my data? Reference standards in superresolution microscopy. *Mol Biol Cell*. 2020 Sep 1;31(19):2093-2096.
- [2] Jimenez A, Friedl K, Leterrier C 'About samples, giving examples: optimized procedures for single molecule localization microscopy' in *Methods* 174, 100–114 (2019).
- [3] Schermelleh L, Ferrand et al. Super-resolution microscopy demystified. *Nat Cell Biol* 21, 72–84 (2019).
- [4] Thompson RE, Larson DR, Webb WW, 'Precise nanometer localization analysis for individual fluorescent probes' in *Biophys Journal* 82. (2002).
- [5] F. Fricke, M. S. Dietz, M. Heilemann 'Single-Molecule Methods to Study Membrane Receptor Oligomerization' in *ChemPhysChem* 2015, 16, 713 – 721.
- [6] K. Bielec, G. Bubak et al. Analysis of Brightness of a Single Fluorophore for Quantitative Characterization of Biochemical Reactions in *Journal Phys. Chem. B* 2020, 124.
- [7] Yan Chen, Li-Na Wei, Joachim D. Mueller, 'Unraveling Protein-Protein Interactions in Living Cells with Fluorescence Fluctuation Brightness Analysis', *Biophysical Journal* Volume 88 June 2005 4366–4377.
- [8] Hellmeier et al. 'DNA origami demonstrate the unique stimulatory power of single pMHCs as T cell antigens', *PNAS* 2021 Vol. 118 No. 4.
- [9] S. Beater et al " in *Methods in Cell Biology*, Volume 123 Elsevier Inc.
- [10] Patrick Macdonald et al. 'Brightness analyses' in *Methods in Enzymology*, Volume 518 Elsevier (2013).

- [11] Y. Chen et al. Probing protein oligomerization in living cells with fluorescence fluctuation spectroscopy. *Proceedings of the National Academy of Sciences of the United States of America*, 100, 15492–15497 (2003).
- [12] Moertelmaier, M., M. Brameshuber, M. Linimeier, G. J. Schütz, and H. Stockinger. Thinning out clusters while conserving stoichiometry of labeling. *Appl Phys Lett* 87:263903 (2005).
- [13] Brameshuber, M. and G. J. Schütz. 2012. Detection and quantification of biomolecular association in living cells using single-molecule microscopy. *Methods in Enzymology* 505: 159-186.
- [14] Brameshuber, M., F. Kellner, B. K. Rossboth, H. Ta, K. Alge, E. Sevsik, J. Göhring, M. Axmann, F. Baumgart, N. R. J. Gascoigne, S. J. Davis, H. Stockinger, G. J. Schütz, and J. B. Huppa. 2018. Monomeric TCRs drive T cell antigen recognition. *Nature Immunology* 19(5):487–496.
- [15] Arun Malhotra 'Tagging for Protein Expression' in *Methods in Enzymology*, Volume 463 (2009)
- [16] Victor A Gault and Neville H McClenaghan, 'Understanding Bioanalytical Chemistry: Principles and Applications', Wiley 2009.
- [17] Bang D, Kent SB. His-6 tag-assisted chemical protein synthesis, in *Proc Natl Acad Sci U S A*. 2005, 102(14):5014-9.
- [18] Smita B. Gunnoo and Annemieke Madder, 'Chemical Protein Modification through Cysteine' in *ChemBioChem* 2016, 17 Wiley VCH 2016.
- [19] <https://www.thermofisher.com/at/en/home/life-science/protein-biology/protein-biology-learning-center/protein-biology-resource-library/pierce-protein-methods/sulfhydryl-reactive-crosslinker-chemistry.html>
- [20] Maximilian H Ulbrich & Ehud Y Isacoff 'Subunit counting in membrane-bound proteins' *NATURE METHODS* VOL.4 NO.4 2007.
- [21] Kubitscheck, *Fluorescence Microscopy: From Principles to Biological Applications*. ISBN 9783527329229 Wiley VCH Verlag (2017).
- [22] Platzer, R., Rossboth, B.K., Schneider, M.C. et al. Unscrambling fluorophore blinking for comprehensive cluster detection via photoactivated localization microscopy. *Nat Commun* 11, 4993 (2020).

- [23] Johannes B. Huppa et al. 'TCR-peptide-MHC interactions in situ show accelerated kinetics and increased affinity. in NATURE Vol 463 18 February 2010.
- [24] Overall, S.A., Toor, J.S., Hao, S. et al. High throughput pMHC-I tetramer library production using chaperone-mediated peptide exchange. Nat Commun 11, 1909 (2020).
- [25] E. Betzig, G. H. Patterson, R. Sougrat, O. W. Lindwasser, S. Olenych, J. S. Bonifacino, M. W. Davidson, J. Lippincott-Schwartz, H. F. Hess, Science 2006, 313, 1642–1645.
- [26] A. Carisey et al. 'Fluorescence Recovery After Photobleaching' Cell Migration: Developmental Methods and Protocols, Methods in Molecular Biology, vol. 769 Springer.
- [27] Edward T. Castellana, Paul S. Cremer, 'Solid supported lipid bilayers: From biophysical studies to sensor design', Elsevier, Surface Science Reports 61, 429–444 (2006).
- [28] Lipowsky, Seifert, 'Adhesion of vesicles and membranes' Mol. Cryst. Liq. Cryst. 202, 17-25 (1991)
- [29] Seifert, 'Configurations of fluids membranes and vesicles' Adv. Phys. 46, 13-137 (1997)
- [30] Schönherr H, Johnson JM, Lenz P, Frank CW, Boxer SG. 'Vesicle Adsorption and Lipid Bilayer Formation on Glass Studied by Atomic Force Microscopy' Langmuir 2004, 20, 26, 11600-11606
- [31] Ralf P. Richter et al. 'Formation of solid-supported lipid bilayers: an integrated view'. Langmuir 2006, 22, 8, 3497-3505
- [32] J. Rädler et al. 'Phenomenology and kinetics of lipid bilayer spreading on hydrophilic surfaces' Langmuir 11, 439- 4548 (1995).
- [33] Cremer, P. S., & Boxer, S. G. 'Formation and spreading of lipid bilayers on planar glass supports' Journal of Physical Chemistry B, 103(13), 2554-2559 (1999).
- [34] Zimm B.H., Bragg J.K., 'Theory of the Phase Transition between Helix and Random Coil in Polypeptide Chains' (1959) J. Chem. Phys. 31, 526–535

- [35] Marsh, Watts, Knowles, 'Cooperativity of the phase transition in single and multibilayer lipid vesicles' *Biochimica et Biophysica Acta*, 465 (1977) 500-514
- [36] Douglas B. Murphy, 'Fundamentals of light microscopy and electronic imaging' John Wiley & sons (2001).
- [37] Jeff W. Lichtman and José Angel Conchello, 'Fluorescence microscopy' VOL.2 NO.12 p.909-919 *NATURE METHODS* (2005).
- [38] Prashant Prabhat and Turan Erdogan, 'perfecting TIRF optics' *BioOPTICS WORLD* (2009) PennWell Corporation.
- [39] <https://www.olympus-lifescience.com/en/microscope-resource/primer/techniques/fluorescence/anatomy/fluoromicroanatomy/>
- [40] Natalie S. Poulter et al., 'The Physical Basis of Total Internal Reflection Fluorescence (TIRF) Microscopy and Its Cellular Applications', in *Advanced Fluorescence Microscopy: Methods and Protocols*, *Methods in Molecular Biology*, vol. 1251 Peter J. Verveer (ed.), Springer Science+Business Media New York (2015)
- [41] Fish, *Total Internal Reflection Fluorescence (TIRF) Microscopy. Current Protocols in Cytometry* (2009)
- [42] Axelrod, D. *Total Internal Reflection Fluorescence Microscopy in Cell Biology. Traffic*, 2, pp.764-774 (2001).
- [43] Denham Simon and Cutchey Deborah, 'Total internal reflection fluorescence microscopy: high contrast images of surface events'. Nikon application note 10.
- [44] Graham-Smith SF, King TA (2000) *Optics and photonics: an introduction*. Wiley, Chichester, UK
- [45] Eugene Hecht. *Optics - Addison Wesley* 2002
- [46] C. M. Dundas et al. 'Streptavidin–biotin technology: improvements and innovations in chemical and biological applications' in *Appl Microbiol Biotechnol* (2013) 97:9343–9353 2013.
- [47] Peter Jomo Walla, *Modern Biophysical Chemistry: Detection and Analysis of Biomolecules*, Second Edition - ISBN 9783527337736 Wiley VCH Verlag GmbH (2014)

- [48] Hughes L. D. et al. 'choose your label wisely: water-soluble fluorophore often interact with lipid bilayers' in PLoS ONE 9(2): e87649 (2014).
- [49] Helmerich, D.A., Beliu, G., Matikonda, S.S. et al. Photoblueing of organic dyes can cause artifacts in super-resolution microscopy. Nat Methods 18, 253–257 (2021).
- [50] Sviatlana Shashkova and Mark C. Leake, 'Single-molecule fluorescence microscopy review: shedding new light on old problems' Bioscience Reports 37 (2017).
- [51] Rumiana Koynova and Boris Tenchov 'Lipids, phase transition of', Wiley encyclopedia of chemical biology, John Wiley and Sons. Inc. (2008).
- [52] M. Rose et al. Lipid Diffusion in Supported Lipid Bilayers: A Comparison between Line-Scanning Fluorescence Correlation Spectroscopy and Single Particle Tracking. A part of: Membranes vol5,4 702-21 (2015).
- [53] Bishara Marina, The effect of mechanical stimulation on the pMHC concentration threshold for activation of murine T cells. (2019) Bachelor's Thesis - Biophysics Group TU Wien.
- [54] Brameshuber M., Schütz J. G. 'In Vivo Tracking of Single Biomolecules: What Trajectories Tell Us About the Acting Forces'. A part of: P. Tinnefeld et al. (eds.), Far-Field Optical Nanoscopy, Springer Ser Fluoresc, Springer-Verlag Berlin Heidelberg (2012)
- [55] Schnell et al. 'Diffusion measured by fluorescence recovery after photobleaching based on multiphoton excitation laser scanning microscopy.' Journal of Biomedical Optics 13(6):064037 (2008).